The Cryosphere Discuss.,
https://doi.org/10.5194/tc-2017-166-AC1, 2017

The Cryosphere Discussions
Open Access
EGU

Interactive comment on "Effects of undercutting and sliding on calving: a coupled approach applied to Kronebreen, Svalbard" *by* Dorothée Vallot et al.

Dorothée Vallot et al.

dorothee.vallot@geo.uu.se

Received and published: 3 November 2017

We first want to thank the referee for the constructive comments. Our answered answers to the questions are detailed below.

General comment:

One of the main conclusions of the paper is that calving rate is controlled by basal sliding. I can see two problems in the methodology that question the validity of this conclusion. First, the friction coefficient inferred using inverse methods with Elmer/Ice has to be scaled down by "some" orders of magnitude when

Printer-friendly version

Discussion paper

used with HiDEM. I didn't understand the justification regarding the different time scales of calving and sliding processes to justify this scaling. The "some orders of magnitude" should be quantified. Is it a constant for the whole domain? Is it the same value (give it) for all simulations? This should be explained much more precisely.

This is a good point and our original text was not well formulated to explain this properly: There is a clear separation of timescales between the velocities of sliding ($\sim$ m/day) and calving ice ($\sim$ m/sec). This means that as long as sliding is slow enough to be negligible during a single calving event, we can change it without much effect on any single calving event. As an approximation we can assume that fast processes are at equilibrium when we consider slower timescales. However, a rescaling speeds up the frequency of calving, and we can thus 'speed up', within reason, the few minutes of HiDEM simulation to effectively model calving which would otherwise take tens of hours or days, and thus be practically impossible to simulate with HiDEM. By applying scaling, the calving events modelled during the simulation of HiDEM (few minutes) correspond to the sum of calving events that would happen during the time scale of sliding. The scaling factor that we use is the same for the whole domain and for all simulations. We use a friction scaling factor for β equal to 10^{-2} (or sliding velocity scaled up by 10^2), and simulations run until calving stops and a new quasi-static equilibrium is reached.

This is now explained in the text (p. 12, lines 10–18): "This means that as long as sliding is slow enough to be negligible during a single calving event, we can change it without much effect on any single calving event. As an approximation we can assume that fast processes are at equilibrium when we consider slower timescales. However, a rescaling speeds up the frequency of calving, and we can thus 'speed up', within reason, the few minutes of HiDEM simulation to effectively model calving which would otherwise take tens of hours or days, and thus be practically impossible to simulate with HiDEM. By applying scaling, the calving events modelled during the simulation of HiDEM (few minutes) correspond to the sum of calving events that would happen

during the time scale of sliding. The scaling factor that we use is the same for the whole domain and for all simulations. We use a friction scaling factor for β equal to 10^{-2} (or sliding velocity scaled up by 10^{2}), and simulations run until calving stops and a new quasi-static equilibrium is reached."

Second, calving rate is a continuous view of calving, as calving is discrete and a calving rate can only be inferred when averaging a number of calving events during a given time. Here, it seems that calving rate is inferred from one simulation of HiDEM and I then suppose that it is inferred from one calving event? Or a limited number of calving events arising during a very short time? Can we deduce a calving rate from that, and then conclude that calving rate is very sensitive to basal sliding?

This is another good point: During one simulation with HiDEM, several calving events are triggered. Calving rate is then inferred from the difference between the initial and final position of the front, after calving has stopped and the glacier has come to rest. This approach is, as the referee points out, dependent on several assumptions, and the error is not easy to estimate. Therefore, the comparison with observed calving rate is very important in order to estimate the validity of this approach. To be clearer, we use "mean volumetric calving rate" instead of just "calving rate". The discussion on basal sliding is based on the comparison between two time steps with the assumptions made in the simulations. Of course, the fact that it is a one-way coupling and that the advance is step-wise and not continuous (due to observation time resolution and modelling limitations) makes the conclusion dependent on these assumptions. We have now changed the text to better explain that the model results regarding basal sliding and calving are valid only under the specific model assumptions.

In Methods/Frontal ablation calculation:

"For the modelled case, during one simulation with HiDEM, several calving events are triggered. Volumetric calving rate is then inferred from the difference between the initial,

F_i^{elmer}, and final position, F_i^{hidem}, of the front, after calving has stopped."

Also, it should be worth verifying that the results are not too strongly dependent on the time step in between two HiDEM simulations. How different are the calving rates obtained by running the HiDEM model every dt, dt/2, dt/4 time step of the Elmer/Ice model?

This is yet another good point that would need further investigation in a fully coupled version. Here we only have observations every 11 days and do not know what happens at dt/2 or dt/4 so it would not be possible to compare. However, we did early test with gradually vanishing sliding and vanishing under-cut. When sliding vanishes, the under-cut determines calving (compare with Benn et al., 2017), and when both vanish, there is typically no calving at all. When comparing HiDEM calving for specified undercuts of different sizes in Benn et al (2017), the results shows that the magnitude of calving increases with undercut size: for small undercuts calving just removes part of the overhang, but for large undercuts calving removes all of the overhang plus additional ice. The mechanisms are different in each case - low-magnitude calving for small undercuts just involves collapse of part of the unsupported overhang, whereas high-magnitude calving for large undercuts involves forward rotation of the whole front around a pivot point located at the base of the undercut cliff. When the time step is changed as the referee suggest above, there are differences, but the overall rate changes stays roughly within $\pm$50%.

We have now changed the following text to better explain this. In Methods/ Calving with first-principles ice fracture model HiDEM

"If the time step is changed, the overall rate change stays roughly within $\pm 50\%$"

In the discussion:

"Because the imposed undercuts are the product of melt during the whole interval between observations, the model results should be treated with caution. Benn et al.

(2017) compared HiDEM calving for specified undercuts of different sizes and showed that calving magnitude increases with undercut size. For small undercuts, calving simply removes part of the overhang, but for large undercuts calving removes all of the overhang plus additional ice. The mechanisms are different in each case: low-magnitude calving for small undercuts occurs through collapse of part of the unsupported overhang, whereas high-magnitude calving for large undercuts involves forward rotation of the whole front around a pivot point located at the base of the undercut cliff. The long time-step intervals (11 or 18 days) between the starting geometry and the HiDEM simulation in the present study might therefore bias the results towards higher calving events. Testing this possibility is beyond the scope of the present paper, but remains an important goal for future research. Despite this caveat, our results compare remarkably well with observations, and yield valuable insights into the calving process."

Minor remarks:

page 2, lines 12-15: The fact that it is untested against observations certainly also apply to the particle models (or you should give a reference in which the particle model is validated against data).

This is true but this is also the subject of the paper: to test HiDEM results against observations. However, the sentence "These are largely untested against observations, and may fail to adequately represent key processes." was not well placed and broke the transition between the former and the next sentence. Therefore we removed it.

page 2, lines 12-15: The distinction between continuous and discrete approaches could be a bit more rigorous and objective. There are also some drawbacks in the particle model that will anyway render its use very difficult for large or long applications.

We gave more details on the discrete models and drawbacks to transition to the next paragraph:

Printer-friendly version

Discussion paper

"These problems can be circumvented using discrete particle models, which represent ice as assemblages of particles linked by breakable elastic bonds. Ice is considered as a granular material and each particle obeys Newton's equations of motion. Above a certain stress threshold, the bond is broken, which allows the ice to fracture. Åström et al. (2013, 2014) showed that complex crevasse patterns and calving processes observed in nature can be modelled using a particle model, the Helsinki Discrete Element Model (HiDEM). Bassis and Jacobs (2013) used a similar particle model and suggested that glacier geometry provides the first-order control on calving regime. However, the drawback of these models is that due to their high computer resource demand, they only can be applied to a few minutes of physical time. A compromise should be found by coupling a continuum model, such as Elmer/Ice, to a discrete model, such as HiDEM, to successively describe the ice as a fluid and as a brittle solid."

page 2, line 22: with the discrete element model HiDEM

Done!

Figure 1: what are the different colours? Especially the white versus grey?

We added more details in the caption:

"Ocean is in blue, bare rock is in red and glacier ice is in white. The grey area represents the Kronebreen glacier system."

page 3, line 10: as shown by Nahrgang et al. (2014) presenting (there are similar problems with the use of brackets for the references all along the manuscript. Please, check this).

We changed it there and at other places.

Figure 2: should be Elmer/Ice not Elmer/ICE to be consistent with the text.

We changed it.

Table 1: give in the first column the number of day = 11d, etc...

Done!

page 6, lines 1-2: here you are mentioning the one-way coupling between HiDEM and Elmer/Ice, and then saying that a completely coupled model would also couple the hydrology and the ice flow. But to be completely coupled, you should add the coupling with the plume model? I would suggest to modify the transition: Also, an improvement could be to calculate the friction...

We add more information as suggested:

"We call this approach a one-way coupling because inputs to the HiDEM are output results from Elmer/Ice and undercutting model but not vice versa. In Elmer/Ice, we use the observed frontal positions. A completely coupled physical model would use the output of the HiDEM, the modelled front position, as input to the ice flow model Elmer/Ice and the undercutting model. It would also calculate the basal friction from a sliding law rather than an inversion. In principle, such an implementation is possible using the same model components as this study."

page 6, line 20: in this part it should be clearly mentioned what is making the front position advance or retreat. Which equation is solved for the front position? Is it a similar to equation (2) and therefore the front is moving as a balance of ice flow and front melting?

The front is advanced by imposing a Lagrangian scheme over a distance equal to the ice velocity multiplied by the time step. We do not account for the melting during the advance because we only have observations at the beginning and the end of each timespan. Instead, we lump frontal melting by applying an undercut after the advance as explained hereafter.

We add this information.

"The front is advanced by imposing a Lagrangian scheme over a distance equal to the ice velocity multiplied by the time step. We do not account for the melting during the

advance because we only have observations at the beginning and the end of each timespan. Instead, we lump frontal melting by applying an undercut after the advance as explained hereafter."

page 7, line 15: on which Grid? The finite element one? Why not solving equation (3) using the finite element method?

It is possible to solve equation (3) using the finite element method but not the D-infinity flow method. Of course, we could have used another subglacial hydrology model but this was not the case for this study. It is the surface runoff grid (100×100 m).

We add this information in the description of the surface runoff and of the flow path calculation:

"Surface runoff is modelled on a 100×100 grid."

"We use the surface runoff grid."

page 7, line 19: I cannot understand what you mean by this last sentence... what is flow accumulation?

A matlab routine is calculating the flow direction from Equation (3) and given D-infinity flow method. The accumulated flow is the sum of all water flowing in a cell from adjacent cells given this flow direction. Each cell is weighted by the surface runoff calculated for the cell.

page 8, line 10: that sea level corresponds to z = 0 is already mentioned above.

We remove the sentence.

page 9, line 5 and after: this part is not clear. What are the reasons for these 3 different treatments should be explained.

The three different treatments depend on the relative position between the observed and modelled front. To explain it better, we added more details before explaining the

Printer-friendly version

Discussion paper

cases:

"When the first discharge occurs, the melt rate calculated with the plume model in 2D is summed for the period of time between t_0 and t_1 and projected to the advanced front $F_1^{elmer}(z=0)$ (advanced from $F_0^{obs}(z=0)$) at the location of the subglacial outlets and ice is removed normal to the front. This yields a new position of the front at depth z below sea level called $F_1^{elmer}(z)$. At the second iteration, t_2, we know where the front would be if there had not been any calving between t_1 and t_2: $F_2^{elmer}(z=0)$, which is the advanced front from the observed position at t_1, $F_1^{obs}(z=0)$. So we can transfer the whole undercut from previous iteration to $F_2^{elmer}(z)$ if $F_1^{obs}(z=0)$ is situated in front of $F_1^{elmer}(z)$ (see Fig. 4b–c). Otherwise, the undercut would have been fully or partly calved away (see Fig. 4b–c). We then apply the new undercut on this new geometry given the melt rates between t_1 and t_2.

At time t_i, the modelled front position at depth z (advanced by Elmer/Ice from the observed front position at t_{i-1}) is $F_i^{elmer}(z)$ and the observed front position is $F_i^{obs}(z=0)$. We advance this observed front with Elmer/Ice during $\Delta t = t_{i+1} - t_i$ to obtain the front position $F_{i+1}^{elmer}(z=0)$ at t_{i+1}. We want to determine $F_{i+1}^{elmer}(z)$ and depth z given the melt rate calculated between t_i and t_{i+1} and the state of the undercut from the previous front $F_i^{elmer}(z)$ updated by the observed front $F_i^{obs}(z=0)$."

page 9, line 11: again, same remark as above: which method? Are you solving a free surface evolution equation for the front? Is the Elmer/Ice model time step also 11 days? This should be specified somewhere.

We do not use Elmer/Ice for the undercutting model and we do not use a free surface evolution equation. We use the front position evolved with Elmer/Ice, $F_i^{elmer}(z=0)$ and apply the undercut on it. We first determine the melt rate during the time period between t_i and t_{i+1} given the accumulated discharge calculated by the hydrology model and using the plume model. Second, we project this melt rate onto the calving front using the method described above.

page 9, line 27: that varies spatially according to the inversion done using Elmer/Ice? Yes, we use the coefficient of friction calculated by the inversion with Elmer/Ice but scaled down as explained after.

page 9, line 32: see my main point. It clearly questions the fact that a calving rate can be inferred from this approach? What does it change if you run HiDEM every two (or half) timestep?

Please, refer to the general comment answer.

page 10, line 4: which complication? As for the "some orders of magnitude", the explanation should be more precise.

The complications induced come from the construction of the ice in HiDEM. It reads an input file with surface, bed and basal ice coordinates. The basal ice different from the bed where there is undercutting. It is not possible to add more ice under this basal ice and create an ice foot. We give more details:

"HiDEM reads a file with surface and bed coordinates on a grid and a file with surface and basal ice (to take into account the undercut) coordinates. When simulating with an undercut at a discharge location and in order to avoid complication in the HiDEM (position of the basal ice), we remove particles below the maximum melt (no ice foot)."

Table 2, last line first column : $C($ ***instead of*** $C_($

Done!

Figure 5: Downstream the front, one would expect zero friction? Are the value on this plot extrapolated? Should be mentioned.

We added more details in the HiDEM description: "In the ocean, the basal friction coefficient is extrapolated downstream of the front and taken equal to the mean of the values further from the terminus in case the ice advances."

Figure 6: I would expect that the discharge increase along the water path and I

don't see this from the plot. On (b), the axis for SD should also start a 0 (and with a continuous curve going to 0 for no discharge).

It does increase but it is maybe not so obvious with the logarithmic color scale. We use this colorscale to highlight the path. We changed the figure according to the comment (Fig. 1 from the answer).

Table 3: how the sum of SD and ND volume compare to the integrated runoff over the basin?

The sum of SD and ND should be actually equal to the integrated runoff over the basin.

Figure 8; what represent the horizontal thin lines in the ocean?

Do you mean in (d) and (e)? It represents the sea level. We add this information in the figure caption. "Horizontal lines in (d, e) represent the sea level for each time step."

page 15, line 6: To my understanding, $a_c^o bs$ doesn't include only calving but also melt at the front? So, it should also be mentioned.

The melt at the front is not included in the calculation of $a_c^o bs$ (see Eq. 4) but shown in am because it is modelled.

Table 4: it should be am and not $a_m^o bs$ in the table? In the legend, I am a bit confused by what you call the tangential ice velocity (tangent to the front?). Isn't it the velocity normal to the front that you mean here? Same in the legend of Fig.9.

This is true, we change to a_m.

We understand the confusion. It is actually normal to the front and tangent to the flow. It depends in which domain we are. Better clarification is given: "[. . .] difference between the tangential (ice flow direction) ice velocity at the front [. . .]"

Figure 11: As you mention in the text that Fig. 11 shows strain rates that ressem-

ble crevasses pattern, would be nice to have an aerial image of the real crevasse pattern? How do you explain the very similar patterns for all simulations inside the domain? What drive these features? And why choosing to plot strain-rates when you could directly plot places where bounds are broken?

We add a crevasse map in Figure 1 (Fig. 2 from the answer. The crevasses form as a result of increasing strain-rate towards the terminus, and as a result of shear strain near margins, which is rather similar in all cases. Strain-rate is better than broken bonds, since strain-rate differentiates between very narrow cracks and wide crevasses.

page 20, line 1: regarding the key role of basal friction, see my main comment

Please, refer to the general comment answer. We also change the whole section 5.2 to:

"Because the imposed undercuts are the product of melt during the whole interval between observations, the model results should be treated with caution. Benn et al. (2017) compared HiDEM calving for specified undercuts of different sizes and showed that calving magnitude increases with undercut size. For small undercuts, calving simply removes part of the overhang, but for large undercuts calving removes all of the overhang plus additional ice. The mechanisms are different in each case: low-magnitude calving for small undercuts occurs through collapse of part of the unsupported overhang, whereas high-magnitude calving for large undercuts involves forward rotation of the whole front around a pivot point located at the base of the undercut cliff. The long time-step intervals (11 or 18 days) between the starting geometry and the HiDEM simulation in the present study might therefore bias the results towards higher calving events. Testing this possibility is beyond the scope of the present paper, but remains an important goal for future research. Despite this caveat, our results compare remarkably well with observations, and yield valuable insights into the calving process.

Firstly, the HiDEM results show that undercutting associated with meltwater plumes is an essential factor for calving during the melt season (t_4 and t_6). Surface melt leads

to the formation of a subglacial drainage system that ultimately releases the water into the ocean from discharge points at the front of the glacier. Simulations without frontal undercutting at these subglacial discharge locations do not agree well with observed frontal positions and mean volumetric calving rates. In contrast, simulations with frontal undercutting reproduce the retreat reasonably well at these locations, particularly where the discharge is high such as at ND. The largest discrepancy between modelled and observed calving is in the region south of SD at t_4. Here, the model predicts calving of a large block, whereas the observed front underwent little change. This largely reflects the rules used for calving in HiDEM: any block that is completely detached from the main ice body is considered as calved, even if only separated by a narrow crack from the rest of the glacier and still sitting at its original position. This is the case for the large 'calved' region south of SD at t4, where the block was completely detached but remained grounded and in situ. If this were to occur in nature, it would not register as a calving event on satellite images. The discrepancy between model results and observations at this locality therefore may be more apparent than real.

Secondly, the model results replicate the observed high calving rates at t_{11}, after the end of the melt season when there is no undercutting. At this time, the observed mean volumetric calving rate is 24.99×10^5 m^3 d^{-1}, which compares well with the HiDEM rate of 28.50×10^5 m^3 d^{-1}. These values are much higher than those at the start of the melt season, when there is also zero undercutting. This contrast can be attributed to the high strain rates in the vicinity of the ice front at t_{11}, which would encourage opening of tensile fractures (Fig. 11). In turn, the high strain rates result from low basal friction (Fig. 5d), likely reflecting stored water at the glacier bed after the end of the melt season. It is possible that geometric factors also play a role in the high calving rates at t_{11}, because the mean ice front height is greater at that time than at t_0, reflecting sustained calving retreat during the summer months, which would have increased longitudinal stress gradients at the front (Benn et al., 2017). This interpretation is supported by experiments $C(g_0, \beta_6, 0)$ and $C(g_6, \beta_0, 0)$, in which the basal friction values are transposed for non-undercut ice geometries at t_0 and t_6. Imposing low friction (β_6) at t_0

produces mean volumetric calving rates similar to (but smaller than) those observed at t_6, whereas imposing high basal friction (β_0) at t_6 produces low volumetric calving rates similar to those observed at t_0. The influence of basal friction on calving rates is consistent with the results of Luckman et al. (2015), who found that a strong correlation exists between frontal ablation rates and ice velocity at Kronebreen when velocity is high. Low basal friction is associated with both high near-terminus strain rates and high velocities, facilitating fracturing and high rates of ice delivery to the front. Our experiments do not include varying fjord water temperature, so we cannot corroborate the strong correlation between frontal ablation and fjord temperature observed by Luckman et al. (2015). However, our results are consistent with their finding that melt-undercutting is a primary control on calving rates, with an additional role played by ice dynamics at times of high velocity."

And a paragraph of the conclusion to:

"Two factors impacting glacier calving are studied here using HiDEM: i) melt-undercutting associated with buoyant plumes; and ii) basal friction, which influences strain rates and velocity near the terminus. The performance of the calving model is evaluated quantitatively by comparing observed and modelled mean volumetric: calving rate and qualitatively by comparing calved regions. Results show that modelled calving rates are smaller than observed values during the melt season in the absence of melt-undercutting, and that there is a closer match with observations if undercutting is included. Additionally, there is good agreement between modelled and observed calving before (t_0) and after (t_{11}) the melt season, when there is no undercutting. Both modelled and observed calving rates are much greater after the melt season than before, which we attribute to lower basal friction and higher strain rates in the near-terminus region at t_{11}. The influence of basal friction on calving rates is corroborated by model experiments that transposed early and late-season friction values, which had a large effect on modelled calving. These results are consistent with the conclusions of Luckman et al. (2015), that melt-undercutting is the primary control on calving at

Printer-friendly version

Discussion paper

Kronebreen at the seasonal scale, whereas dynamic factors are important at times of high velocity (i.e. low basal friction)."

page 22, line 7: Elmer/Ice.

Done!

References

Åström, J. A., Riikilä, T. I., Tallinen, T., Zwinger, T., Benn, D., Moore, J. C., and Timonen, J.: A particle based simulation model for glacier dynamics, Cryosphere, 7, 1591–1602, doi: 10.5194/tc-7-1591-2013, 2013.

Åström, J. A., Vallot, D., Schäfer, M., Welty, E. Z., O'Neel, S., Bartholomaus, T., Liu, Y., Riikilä, T., Zwinger, T., Timonen, J., et al.: Termini of calving glaciers as self-organized critical systems, Nature Geoscience, 7, 874–878, doi:10.1038/NGEO2290, 2014.

Bassis, J. and Jacobs, S.: Diverse calving patterns linked to glacier geometry, Nature Geoscience, 6, 833–836, doi:10.1038/ngeo1887, 2013.

Benn, D. I., Åström, J., Zwinger, T., Todd, J., Nick, F. M., Cook, S., Hulton, N. R., and Luckman, A.: Melt-under-cutting and buoyancy-driven calving from tidewater glaciers: new insights from discrete element and continuum model simulations, Journal of Glaciology, pp. 1–12, doi:10.1017/jog.2017.41, 2017.

Luckman, A., Benn, D. I., Cottier, F., Bevan, S., Nilsen, F., and Inall, M.: Calving rates at tidewater glaciers vary strongly with ocean temperature, Nature communications, 6, doi: 10.1038/ncomms9566, 2015.

Interactive comment on The Cryosphere Discuss., https://doi.org/10.5194/tc-2017-166, 2017.

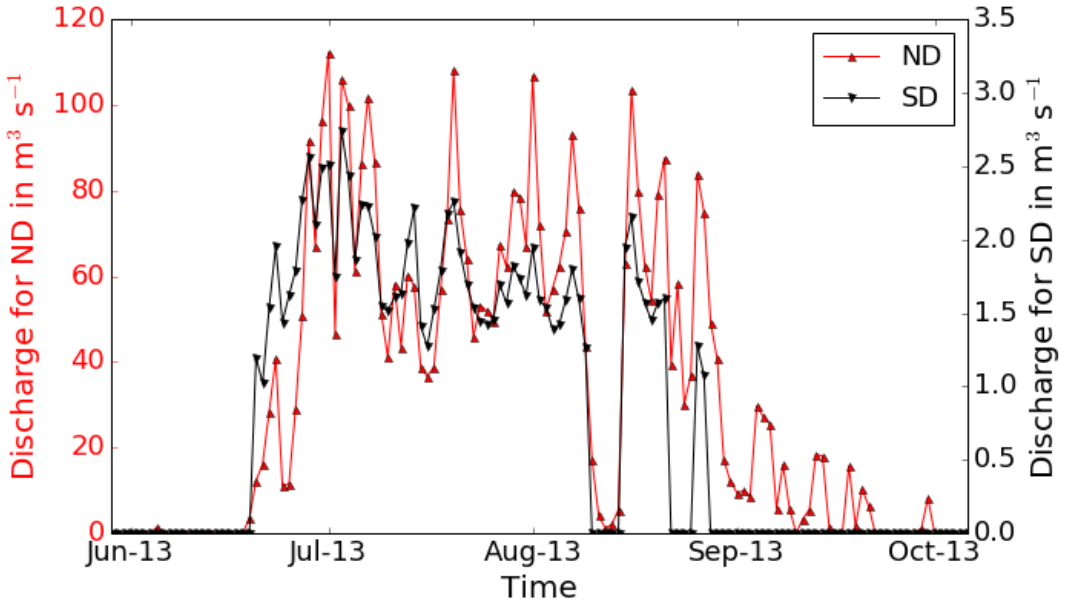

Fig. 1.

Printer-friendly version

Discussion paper

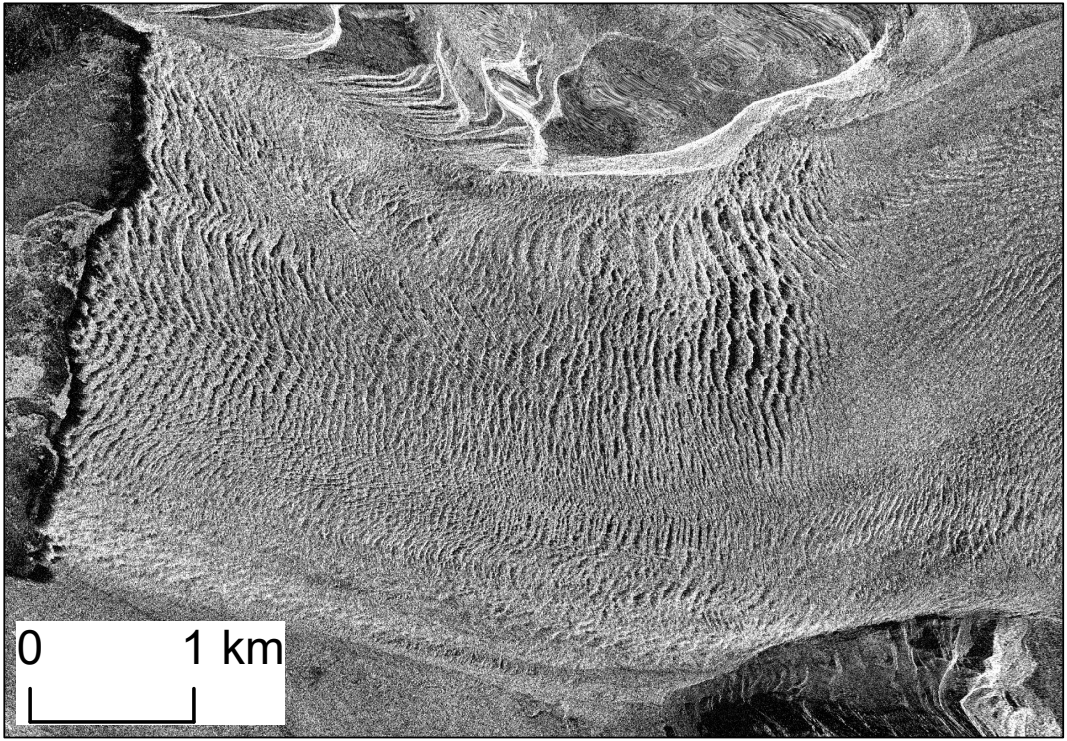

Fig. 2.

The Cryosphere Discuss.,
https://doi.org/10.5194/tc-2017-166-AC2, 2017

The Cryosphere Discussions
Open Access
EGU

Interactive comment on "Effects of undercutting and sliding on calving: a coupled approach applied to Kronebreen, Svalbard" *by* Dorothée Vallot et al.

Dorothée Vallot et al.

dorothee.vallot@geo.uu.se

Received and published: 3 November 2017

We first want to thank the referee for the constructive comments. Our answers to the questions are as follows.

Major comment:

The title of this paper and subsequent references to "coupling"are misleading. There is no coupling performed in this model. The different models used to represent the calving front processes are put together and outputs from one model are inputs of other models, but there is no coupling. Fig. 2 illustrates this very

Printer-friendly version

Discussion paper

well: arrows all have the same direction and outputs from HiDEM are never used as inputs for other models. What this paper does is provide a comprehensive approach to the question of calving, and I think a title using "global approach" or something similar would be more accurate.

This is true and that is why we referred to it as a one-way coupling throughout the text. However, and the referee is right, the title is misleading and we change it to the suggestion: "Effects of undercutting and sliding on calving: a global approach applied to Kronebreen, Svalbard"

As mentioned above, the conclusions separating the impact of geometry, basal sliding and undercutting are not well supported by the results provided. Looking at Fig. 10, it seems that all parameters have an impact on both the location and extend of retreat, but they cannot be clearly distinguished without further experiments. It is true that more experiments are always better and we understand that the conclusion should acknowledge the fact that they are only valid for these cases. However, we do not agree with the statement in the summary "the impact of the basal friction on Fig. 10 (a and c only show the impact of friction) is not clear, as the calving rate is not very different for the high and low friction scenarios, and adding undercutting (Fig. 10c) has an impact similar to changing basal friction." Fig. 9 shows that there are large differences between calving rates when geometry is kept unchanged and basal sliding is changing. Of course more experiments would give a better picture but should be made in a smaller scale so that the cost of running the HiDEM is not as high. We have rewritten the discussion and the conclusion to express our results in a clearer way:

In the discussion:

"Because the imposed undercuts are the product of melt during the whole interval between observations, the model results should be treated with caution. Benn et al. (2017) compared HiDEM calving for specified undercuts of different sizes and showed that calving magnitude increases with undercut size. For small undercuts, calving

simply removes part of the overhang, but for large undercuts calving removes all of the overhang plus additional ice. The mechanisms are different in each case: low-magnitude calving for small undercuts occurs through collapse of part of the unsupported overhang, whereas high-magnitude calving for large undercuts involves forward rotation of the whole front around a pivot point located at the base of the undercut cliff. The long time-step intervals (11 or 18 days) between the starting geometry and the HiDEM simulation in the present study might therefore bias the results towards higher calving events. Testing this possibility is beyond the scope of the present paper, but remains an important goal for future research. Despite this caveat, our results compare remarkably well with observations, and yield valuable insights into the calving process.

Firstly, the HiDEM results show that undercutting associated with meltwater plumes is an essential factor for calving during the melt season (t_4 and t_6). Surface melt leads to the formation of a subglacial drainage system that ultimately releases the water into the ocean from discharge points at the front of the glacier. Simulations without frontal undercutting at these subglacial discharge locations do not agree well with observed frontal positions and mean volumetric calving rates. In contrast, simulations with frontal undercutting reproduce the retreat reasonably well at these locations, particularly where the discharge is high such as at ND. The largest discrepancy between modelled and observed calving is in the region south of SD at t_4. Here, the model predicts calving of a large block, whereas the observed front underwent little change. This largely reflects the rules used for calving in HiDEM: any block that is completely detached from the main ice body is considered as calved, even if only separated by a narrow crack from the rest of the glacier and still sitting at its original position. This is the case for the large 'calved' region south of SD at t4, where the block was completely detached but remained grounded and in situ. If this were to occur in nature, it would not register as a calving event on satellite images. The discrepancy between model results and observations at this locality therefore may be more apparent than real.

Secondly, the model results replicate the observed high calving rates at t_{11}, after the

Printer-friendly version

Discussion paper

end of the melt season when there is no undercutting. At this time, the observed mean volumetric calving rate is $24.99 \times 10^5\,\mathrm{m^3\,d^{-1}}$, which compares well with the HiDEM rate of $28.50 \times 10^5\,\mathrm{m^3\,d^{-1}}$. These values are much higher than those at the start of the melt season, when there is also zero undercutting. This contrast can be attributed to the high strain rates in the vicinity of the ice front at t_{11}, which would encourage opening of tensile fractures (Fig. 11). In turn, the high strain rates result from low basal friction (Fig. 5d), likely reflecting stored water at the glacier bed after the end of the melt season. It is possible that geometric factors also play a role in the high calving rates at t_{11}, because the mean ice front height is greater at that time than at t_0, reflecting sustained calving retreat during the summer months, which would have increased longitudinal stress gradients at the front (Benn et al., 2017). This interpretation is supported by experiments $C(g_0, \beta_6, 0)$ and $C(g_6, \beta_0, 0)$, in which the basal friction values are transposed for non-undercut ice geometries at t_0 and t_6. Imposing low friction (β_6) at t_0 produces mean volumetric calving rates similar to (but smaller than) those observed at t_6, whereas imposing high basal friction (β_0) at t_6 produces low volumetric calving rates similar to those observed at t_0. The influence of basal friction on calving rates is consistent with the results of Luckman et al. (2015), who found that a strong correlation exists between frontal ablation rates and ice velocity at Kronebreen when velocity is high. Low basal friction is associated with both high near-terminus strain rates and high velocities, facilitating fracturing and high rates of ice delivery to the front. Our experiments do not include varying fjord water temperature, so we cannot corroborate the strong correlation between frontal ablation and fjord temperature observed by Luckman et al. (2015). However, our results are consistent with their finding that melt-undercutting is a primary control on calving rates, with an additional role played by ice dynamics at times of high velocity."

In the conclusion:

"Two factors impacting glacier calving are studied here using HiDEM: i) melt-undercutting associated with buoyant plumes; and ii) basal friction, which influences

strain rates and velocity near the terminus. The performance of the calving model is evaluated quantitatively by comparing observed and modelled mean volumetric: calving rate and qualitatively by comparing calved regions. Results show that modelled calving rates are smaller than observed values during the melt season in the absence of melt-undercutting, and that there is a closer match with observations if undercutting is included. Additionally, there is good agreement between modelled and observed calving before (t_0) and after (t_{11}) the melt season, when there is no undercutting. Both modelled and observed calving rates are much greater after the melt season than before, which we attribute to lower basal friction and higher strain rates in the near-terminus region at t_{11}. The influence of basal friction on calving rates is corroborated by model experiments that transposed early and late-season friction values, which had a large effect on modelled calving. These results are consistent with the conclusions of Luckman et al. (2015), that melt-undercutting is the primary control on calving at Kronebreen at the seasonal scale, whereas dynamic factors are important at times of high velocity (i.e. low basal friction).

In this paper, we have shown that one-way coupling of ice-flow, surface melt, basal drainage, plume-melting, and ice-fracture models can provide a good match to observations and yield improved understanding of the controls on calving processes. Full model coupling, including forward modelling of ice flow using a physical sliding law, would allow the scope of this work to be extended farther, including prediction of glacier response to atmospheric and oceanic forcing."

It is not clear if all the 11 time steps described in Tab. 1 are modeled, or if only a subset of these times are used. Results from t0 , t4 , t6 and t11 are mostly presented, but Fig. 10 also shows results at different time steps.

The 11 time steps in Table 1 are used to model undercutting. We use all observations/modelled data (front position/runoff) to assess the undercutting for each time step. Thereafter, when using the particle model, we only model four time steps (t_0, t_4, t_6 and t_{11}) for their particularity as the comment in Table 1 shows.

To explain our strategy clearly, we changed a whole paragraph in this section based on the line by line comments which can help readers to understand how each model is separated:

"First, we infer sliding at each time step from surface velocities using an adjoint inverse method implemented in Elmer/Ice with an updated geometry from observations at different time steps. At each iteration, i, corresponding to an observed front position, F_i^{obs}, the front and the surface are dynamically evolved during the observation time (roughly 11 days) with Elmer/Ice. By the end of the time step, the front has advanced to a new position, F_{i+1}^{elmer}. Here we use $i+1$ because this is the position the front would have at t_{i+1} in the absence of calving. Second, given subglacial drainage inferred from modelled surface runoff, a plume model calculates melt rates based on the subglacial discharge for each iteration, which are subsequently applied to the front geometry at subglacial discharge locations. At each iteration, the front geometry takes into account the undercut modelled at the former iteration. Finally, the sliding, geometry and undercut (when applicable) are taken as input to the calving particle model HiDEM for each iteration and a new front, F_{i+1}^{hidem}, is computed for four iterations, t_0, t_4, t_6, t_{11}, which represent interesting cases (see comments on Table 1). More details about each aspect of the model process are given in the following sections."

What is the rational for keeping or removing the undercut in one case or another when the ice front advances or retreats (Fig. 4 and p.9)? Some explanations justifying these choices should be added as opposed to presenting the choices made without any justification. I cannot quite figure out why the undercut from the previous profile is not always considered.

The idea is to take into consideration the observations. One should keep in mind that the undercut estimation is done independently from the HiDEM simulations. The first iteration undercut is estimated from the advanced front, F_1^elmer (advanced from F_0^obs), by projecting daily melt rate during the time period t_1–t_0. At the second iteration, t_2, we know where the front would be if there had not been any calving between t_1 and t_2:

F_2^elmer, which is the advanced front from the observed position at t_1, F_1^obs. So we can transfer the whole undercut from previous iteration to F_2^elmer if F_1^obs is situated in front of F1elmer (case a). Otherwise, the undercut would have been fully or partly calved away (case b and c). We then apply the new undercut on this new geometry given the melt rates between t_1 and t_2.

We changed the text in consequence:

"When the first discharge occurs, the melt rate calculated with the plume model in 2D is summed for the period of time between t_0 and t_1 and projected to the advanced front $F_1^{elmer}(z=0)$ (advanced from $F_0^{obs}(z=0)$) at the location of the subglacial outlets and ice is removed normal to the front. This yields a new position of the front at depth z below sea level called $F_1^{elmer}(z)$. At the second iteration, t_2, we know where the front would be if there had not been any calving between t_1 and t_2: $F_2^{elmer}(z=0)$, which is the advanced front from the observed position at t_1, $F_1^{obs}(z=0)$. So we can transfer the whole undercut from previous iteration to $F_2^{elmer}(z)$ if $F_1^{obs}(z=0)$ is situated in front of $F_1^{elmer}(z)$ (see Fig. 4b–c). Otherwise, the undercut would have been fully or partly calved away (see Fig. 4b–c). We then apply the new undercut on this new geometry given the melt rates between t_1 and t_2.

At time t_i, the modelled front position at depth z (advanced by Elmer/Ice from the observed front position at t_{i-1}) is $F_i^{elmer}(z)$ and the observed front position is $F_i^{obs}(z=0)$. We advance this observed front with Elmer/Ice during $\Delta t = t_{i+1} - t_i$ to obtain the front position $F_{i+1}^{elmer}(z=0)$ at t_{i+1}. We want to determine $F_{i+1}^{elmer}(z)$ and depth z given the melt rate calculated between t_i and t_{i+1} and the state of the undercut from the previous front $F_i^{elmer}(z)$ updated by the observed front $F_i^{obs}(z=0)$."

Line by line comments:

p.1 l.17: "rigorous methods": the problem is not so much about rigorous methods but more about some processes impacting calving that we still don't understand, as well as small scale features (mm long cracks) that cannot be observed

and included in models.

We change to:

"To a large degree, this uncertainty reflects the limited understanding of processes impacting calving from tidewater glaciers and ice shelves, and associated feedbacks with glacier dynamics. In particular, calving occurs by the propagation of fractures, which are not explicitly represented in the continuum models used to simulate ice flow and glacier evolution."

p.1 l.20: "impacting on submarine melt rate" → ***"impacting submarine melt rate"***

Done!

p.2 l.1: "during the summer and the autumn" → ***"during summer and autumn"***

Done!

p.2 l.3: "followed by ice-front collapse": not clear

We change to: "triggering collapse of the ice above"

p.2 l.12: The problem is actually not so much the representation of calving in models but the processes impacting calving that are not enough understood and therefore cannot be included into models.

We change to: "In addition to the lack of process understanding, continuum models cannot explicitly model fracture, but must use simple parameterisations such as damage variables or phenomenological calving criteria."

p.2 l.16: Again here, it is not really coupling but feeding the particule model with appropriate inputs from Elmer/Ice.

This is true and that is why the word "introduce" is used because it is just an introduction. But we agree that it is misleading. Therefore, we change to:

"In this paper, we use both the capabilities of the continuum model Elmer/Ice and the

discrete element model HiDEM."

p.2 l.32: "one of the fastest"** → **"one of the fastest glacier"

Done!

p.2 l.33: How much seasonal variation is this glacier experiencing?

See question below.

p.3 l.3: How large are the seasonal variations? What is the velocity in winter?

We add more information: "In 2013, averaged velocities close to the front ranged from 2.2 to 3.8 $\mathrm{m\,d^{-1}}$ in the summer and fell to 2 $\mathrm{m\,d^{-1}}$ directly after the melt season. In 2014, however, they stayed relatively high (around 4 $\mathrm{m\,d^{-1}}$) throughout the summer and progressively fell to 3 $\mathrm{m\,d^{-1}}$ in the winter."

p.3 Fig.1: Consider adding Kongsfjorden on the figure. Calving front position for 16 Octobre 2013 is not visible, consider changing it.

Done!

p.3 l.10 "by (Nahrgang et al., 2014)"** → **"by Nahrgang et al. (2014)"

Done!

p.3 l.11-15: Past tense should be used to describe measurements made in 2013.

Done!

p.3 l.11-15: How representative of the seasonal cycle are these values?

These values are only valid for the summer season.

p.4 Fig.2: There is no feedback and therefore no coupling shown on this figure. Outputs from one model are used as parameters/inputs for the next model.

We therefore refer to it as a one-way coupling approach. We change the first sentence

of the section though to:

"We use surface velocity and frontal position data described above to test the effects of sliding and undercutting on calving using different models in a global approach."

p.4 l.7: What about the other observations (geometry, ice temperature and viscosity)? Where do they come from?

Geometry was described in section 3.3 but we agree that all observations should be presented together so we moved it and changed the title of the section to "3.1. Observed geometry, surface velocities and front positions". There is no observation of ice temperature or viscosity and more details on the Elmer/Ice model description is given in Vallot et al. (2017), cited in section 3.3. To be clear, we added this information: "More details on the model (viscosity, ice temperature, inversion time-steps, etc.) are given in Vallot et al. (2017)."

p.5 l.6: Is the sliding inverted just at the beginning of the simulation or recomputed for each time step? In this case how is the change in the glacier geometry computed (or maybe observations are used)?

The sliding is inverted at each time step given the observations (velocity, topography, front position). Thereafter the surface elevation is relaxed using Eq. 2 in a transient simulation. This new surface is then used in the next iteration. This is done independently of the HiDEM and is only using front position observation. This is what should change in a full coupling. To avoid confusion, we add "at each time step".

p.5 l.9: How are the front and surface evolved? Are they run from the previous iteration and therefore the 12 time steps are run with the model? In this case, why only show results for 6 cases and not the entire melt season? If not, how are the front and surface evolved? Also, modeling ice front changes in ice flow model is not an easy task and is currently the subject of active research. How is the front evolved with the Elmer/Ice model? There is no reference or explanation of

how the ice front migrates and no Elmer/Ice paper describing such an evolution to my knowledge. This has to be better explained.

The front and surface are evolved in a transient simulation using Elmer/Ice, as explained in the following section (3.3). We add more information on the front evolution:

"The front is advanced by imposing a Lagrangian scheme over a distance equal to the ice velocity multiplied by the time step. We do not account for the melting during the advance because we only have observations at the beginning and the end of each timespan. Instead, we lump frontal melting by applying an undercut after the advance as explained hereafter."

Since it is not a full coupling, the results from the HiDEM are not used in Elmer/Ice where we only use front position observation. This section was intended to be more a presentation of the modelling concept with more explanation to follow. Is it misleading? We add a sentence referring to the next paragraphs for more details:

" More details about each aspect of the model process are given in the following sections."

Also, the sentence about the front and surface evolution is misleading since it seems that the front evolves from one observation to another, which is not the case. So we change it to:

"the front and the surface are dynamically evolved during the observation time"

p.6 l.1: "coupling": same as above

Here we explain that we use "one-way coupling" with input from a model is output from another but not vice-versa.

p.6 l.1: If the front position is not used as inputs for the Elmer/Ice initial front position, what is used then?

We use the observed frontal position for Elmer/Ice simulations. We add this informa-

tion: "In Elmer/Ice, we use the observed frontal positions."

p.6 Eq. 1: Consider using vectors. Also u is used both here for the velocity, and later (e.g. Tab. 2) for the undercutting. Change one or the other.

Thank you for this suggestion! We chose to change the velocity to v and we change to vectors.

p.6 l.8: Again here, is the friction optimized at each time step or just at the beginning of the simulation?

The friction is optimised at each time step for which we have observations. We add this information: "The basal friction coefficient, β, is optimized at each time step to best reproduce observed velocity distribution at the surface of the glacier as described in Vallot et al. (2017)."

p.6 l.9: "the self-adjointness" $\rightarrow$ ***"a self-adjoint algorithm"***

Done!

p.6 l.10 and l.11: Consider adding older references that first used such methods.

We add references:

"This is done by using a self-adjoint algorithm of the Stokes equations for an inversion (e.g. Morlighem et al., 2010; Goldberg and Sergienko, 2011; Gillet-Chaulet et al., 2012) and implemented in Elmer/Ice (Gagliardini et al., 2013)."

p.6 l.13: This paragraph could be put in the data section (section 3.1) to improve consistency.

Done!

p.6 l.20: "The front position is also able to advance": How is it able to advance? See point above

As described above, we add the information: "The front is advanced by imposing a

Lagrangian scheme over a distance equal to the ice velocity multiplied by the time step."

p.6 l.20: "$F_i^obs(0)$": I would imagine that observations show the front position on the surface of the glacier and not at sea level.

We assume that the front is vertical above sea level. We add this information: "We assume that the front is vertical above the sea level so that the observed front position (at the surface of the glacier) is the same at sea level."

p.6 l.20-21: There are several front positions observed and computed. The authors should start by listing all the front position computed (F^elmer, F^HiDEM, ...) and explaining where they come from. That might be something to add on Fig.2.

Thank you for the suggestion! We added this information in the section 3.2:

"First, we infer sliding at each time step from surface velocities using an adjoint inverse method implemented in Elmer/Ice with an updated geometry from observations at different time steps. At each iteration, i, corresponding to an observed front position, F_i^{obs}, the front and the surface are dynamically evolved during the observation time (roughly 11 days) with Elmer/Ice. By the end of the time step, the front has advanced to a new position, F_{i+1}^{elmer}. Here we use $i+1$ because this is the position the front would have at t_{i+1} in the absence of calving. Second, given subglacial drainage inferred from modelled surface runoff, a plume model calculates melt rates based on the subglacial discharge for each iteration, which are subsequently applied to the front geometry at subglacial discharge locations. At each iteration, the front geometry takes into account the undercut modelled at the former iteration. Finally, the sliding, geometry and undercut (when applicable) are taken as input to the calving particle model HiDEM for each iteration and a new front, F_{i+1}^{hidem}, is computed for four iterations, t_0, t_4, t_6, t_{11}, which represent interesting cases (see comments on Table 1). More details about each aspect of the model process are given in the following sections."

F^obs and F^elmer are already in Fig. 2.

p.6 section 3.3: What is the resolution (horizontal and vertical) of the model, especially close to the ice front? What are the time steps used for the continuum model?

We add this information:

"We use an unstructured mesh, with spatial repartition of elements based on the mean observed surface velocities in the horizontal plane (roughly 30 m resolution close to the front). Vertically, the 2D mesh is extruded with ten levels (roughly 10 m resolution close to the front)."

Later in the section (after the surface equation), we add:

"We use a time step of 1 day."

p.7 l.8: convention for the reference (twice)

Corrected!

p.7 l.29: "five kilometers" → "five kilometers away"

Done!

p.8 l.1: How long does it take to reach a steady-state?

We have clarified this in the text, p.8 l.1 now reads: "The model is spun-up for 1000 model seconds until the turbulent kinetic energy in the region of the plume reaches a steady state..."

p.8 l.4-7: So my understanding is that the discharge varies but not the ocean conditions. Ocean conditions are reported quite accurately on p.3, so why not use these conditions instead of uniform ambiant ocean properties? Also, in all these cases, the ice front is assumed to be vertical, why not try cases with pre-existing undercutting? I understand that it might not be possible to test all these

cases, but at least assessing the uncertainty caused by such assumptions would be important.

The model uses temperature and salinity profiles collected from Kongsfjorden, as described on p7. l.26–30. They are uniform in the sense that the same conditions were used in the different discharges tested, we have rewritten to clarify this. Edited p.8. l.5 to "Instead, representative cases M_d using the ambient ocean properties described above and discharges d of 1, 10, 50 and 100 $m^3 s^{-1}$ were tested and the melt rate profiles for intermediate discharges were linearly interpolated from these cases."

The reasons for and implications of not varying the ocean properties and the ice front angle are discussed in Section 5.1. However, it is important to give the full picture and we have replaced the paragraph on ocean variability in the discussion (p.19 l.3-12) with the paragraph below:

"By using ambient temperature and salinity profiles that do not vary in time, we neglect the inter- and intra-annual variability in Kongsfjorden. This variability can affect the calculated melt rate in two ways: i) the three-equation melt parameterisation explicitly includes the temperature and salinity at the ice-face, and ii) the ambient stratification affects the vertical velocity and neutral buoyancy height of the plume. The direct effect of changes in temperature and salinity on the melt equations are well tested. Past studies using uniform ambient temperature and salinity conditions have found a linear relationship between increases in ambient fjord temperatures and melt rates, with the slope of the relationship dependent upon the discharge volume (Holland et al., 2008b; Jenkins, 2011; Xu et al., 2013). Salinity, on the other hand, has been shown to have a negligible effect on melt rates (Holland et al., 2008a). However, with a non-uniform ambient temperature and salinity, the effects of changes in the stratification on the plume vertical velocity and neutral buoyancy are much more complex. The stratification in Kongsfjorden is a multi-layer system, with little or no direct relationship between changes in different layers (Cottier et al., 2005). Therefore, testing cases by uniformly increasing or decreasing the salinity would not be informative for understanding the true effects of

inter- and intra-annual variability. The high-computational expense of the plume model used here means that it is not yet feasible to run the model on the timescales necessary to understand this variability, nor to run sufficient representative profiles to provide a useful understanding of the response. Previous work has suggested that intra-annual changes in the ambient stratification are small enough that plumes are relatively insensitive to these changes (Slater et al., 2017) and that plume models forced with variations in runoff and a constant ambient stratification can qualitatively reproduce observations (Stevens et al., 2016). For these reasons, we highlight this as a limitation of the current implementation, and suggest that this should be addressed in future investigations of plume behaviour. A model based upon one-dimensional plume theory (e.g. Jenkins, 2011; Carroll et al., 2015; Slater et al., 2016) would be less computationally expensive and may allow some of these limitations to be addressed. However, such a model would not capture the strong surface currents driven by the plume which are important for the terminus morphology studied here."

p.9 l.6-10: What is the rational for keeping or removing the undercut in one case or another? Some explanations justifying these choices should be added.

See answer to major comment.

p.9 l.19: How many broken beams are added and how was this number chosen? What is the impact of increasing or reducing this number on the results? Also does the number of broken beams increase during the melt season as the ice gets more damaged?

This must be some kind of misunderstanding on how the model is constructed - we do not add broken beams at any point. What the referee probably refers to is the small fraction of broken beams at the beginning of the simulation. As long as this fraction is small and broken beams are spatially uncorrelated it has only a minor influence on calving. It is a good suggestion by the referee to increase this fraction to mimic melt and to investigate how that would affect calving. However, in our opinion it would not

Printer-friendly version

Discussion paper

be useful to add even more results to this paper and yet another calving variable in a model which already has a lot.

p.9 l.30: How long is the HiDEM model run for at each time step? And how long does it take to run it?

We add this information: " The model run for 100 s, which takes two days of simulation physical time."

p.10 l.2: What kind of instabilities are developing and why?

We add more information to make this statement clearer:

"HiDEM reads a file with surface and bed coordinates on a grid and a file with surface and basal ice (to take into account the undercut) coordinates. When simulating with an undercut at a discharge location and in order to avoid complication in the HiDEM (position of the basal ice), we remove particles below the maximum melt (no ice foot)."

p.10 l.7-11: What is the rational for decreasing the friction? How is the choice of friction impacting your results?

There is a clear separation of timescales between the velocities of sliding ($\sim$m/day) and calving ice ($\sim$m/sec). This means that as long as sliding is slow enough to be negligible during a single calving event, we can change it without much effect on any single calving event. As an approximation we can assume that fast processes are at equilibrium when we consider slower timescales. However, a rescaling speeds up the frequency of calving, and we can thus 'speed up', within reason, the few minutes of HiDEM simulation to effectively model calving which would otherwise take tens of hours or days, and thus be practically impossible to simulate with HiDEM. By applying scaling, the calving events modelled during the simulation of HiDEM (few minutes) correspond to the sum of calving events that would happen during the time scale of sliding. The scaling factor that we use is the same for the whole domain and for all simulations. We use a friction scaling factor for β equal to 10^{-2} (or sliding velocity scaled up by 10^2),

and simulations run until calving stops and a new quasi-static equilibrium is reached. This is now better explained in the text:

"There is a clear separation of timescales between the velocities of sliding ($\sim$m day^{-1}) and calving ice ($\sim$m sec^{-1}). This means that as long as sliding is slow enough to be negligible during a single calving event, we can change it without much effect on any single calving event. As an approximation we can assume that fast processes are at equilibrium when we consider slower timescales. However, a rescaling speeds up the frequency of calving, and we can thus 'speed up', within reason, the few minutes of HiDEM simulation to effectively model calving which would otherwise take tens of hours or days, and thus be practically impossible to simulate with HiDEM. By applying scaling, the calving events modelled during the simulation of HiDEM (few minutes) correspond to the sum of calving events that would happen during the time scale of sliding. The scaling factor that we use is the same for the whole domain and for all simulations. We use a friction scaling factor for β equal to 10^{-2} (or sliding velocity scaled up by 10^2), and simulations run until calving stops and a new quasi-static equilibrium is reached."

p.10 l.19: It should be mentioned that this is volumetric ablation rate (same for volumetric calving rate in the rest of the paper). Many people use calving/ablation rate as changes per unit area (in m/yr), which can be confusing.

We add "mean volumetric" in front of ablation rate and calving rate in the whole paper.

p.10 l.20: Integrals over Gamma usually refer to contour intervals and not surface integrals, using S or Σ instead would be more consistent with literature.

Thank you for the suggestion. We change Γ for Σ.

p.10 Eq.5: What is $z\Gamma_w$?

This was meant to be the vertical dimension of (now) Σ. We change it to $z \in \Sigma$.

p.10 l.28: "parameterisations" $\rightarrow$ "parameters"

Done!

p.10 l.30: u was already used for velocity (see above)

We change the velocity for v and kept u for undercut (see above).

p.10 l.30: Only 4 time steps are mentioned here. What happens to the other ones, are they just excluded? In this case, what is used for the prior undercut?

Undercuts are computed from for each timestep for which there are observations, so independently from theand HiDEM simulations were conducted for four time steps (t_0, t_4, t_6, and t_{11}). This is now clearly expressed in the text and Tables.

p.11 l.1: Only a subset of $(i, j) \in [0, 4, 6, 11]$ ***is covered, not accurate.***

We remove this.

p.11 l.6: configuration C_k ***is not defined and not used anywhere else, should be consistent with the rest of the paper***

That is right. We changed the names of the configurations at a later stage but the table had not been updated. This is now done!

p.11 Tab. 2: Configuration is here a function of time (t_i) ***as opposed to geometry*** (g_i) ***in the rest of the paper***

See above.

p.12 Fig.6 caption: "data gaps corresponds" $\rightarrow$ ***"data gaps correspond"***

Done!

p.13 l.Tab.3: Discharged should be provided in m3/s to be consistent with the rest of the text. No data between t_{10} ***and*** t_{11} ***, this should be added even if the values are just zero. Also, how are the melting rates for each case computed based on Fig.7? Is an interpolation between the four cases been performed? Or something else?***

In Table 3, we wanted to show the total volume discharged during the time period, hence a volume in m3. However, if it is irrelevant, we could provide an averaged discharge in m3/s. Wee added t_{10} to t_{11}. Yes, melting rates are interpolated from the four cases and this is mentioned in section 3.5:

"discharges d of 1, 10, 50 and 100 $\mathrm{m^3\,s^{-1}}$ were tested and the melt rate profiles for intermediate discharges were linearly interpolated from these cases"

p.13 Fig.7: How different are the results if there is undercut introduced in the geometry?

We discuss the impacts of this in Section 5.1. Slater et al. (2017) show that undercuts only have a weak effect on plume dynamics, and therefore our projection of the melt rates onto the terminus is a reasonable way to address this, based on research to date. This is an area which requires further investigation with high-resolution plume models; however, as this is not the primary focus of this paper we suggest that once other studies have addressed this, their results, models and methodologies can be incorporated into future development of the approach we present here.

P.14 Fig.8: It is the only time in the paper, where results from times other than t0 , t4 , t6 and t11 are presented. Are the other time steps computed? And what is the rational to only present some ice front positions here?

The undercut estimation from melt rates is independent from the HiDEM simulations. We use daily runoff and observed front positions for it. So in order to get the undercut for t_6, we need to know the undercut state from previous steps. We do not present the front positions after t_6 since we do not use them for the HiDEM simulations. For t_{11}, we consider the front vertical (the remained undercut from last iteration with melt being calved away).

p.14 Fig.8: If z is the height above sea level, Fig.8 b and c are for z = -3m and z = -42m, and the stars in Fig.8 d and e indicate the plan view elevation, why are

the start not aligned at the same height on Fig.8 d and e? Also it might be more clear to use "Elevation from sea level" or something similar instead of "Distance to the bed" on Fig.8 d and e as this is what is used in the rest of the figure.

The stars are not aligned because the sea level is actually not at the same position compared to bed elevation for each iteration. We chose to use "distance to bed" instead of "elevation from sea level" because the plume starts at the bed elevation and we wanted to compare from there.

p.14 l.11: What do the authors mean by "smoother"?

We mean the undercut is not as abrupt as ND: We change the sentence to:

"In the first 50 m from the surface, the undercut at the SD is not as abrupt as at the ND and is also smaller"

p.14 l.12: "stretching" $\rightarrow$ ***"stretches"***

Done!

p.15 l.2: Why not do it more often? How long does it take to run the model?

The runoff is available everyday and thus the discharge. Undercutting is therefore applied everyday based on the observed front position. Unfortunately, we only have observed front every 11 days and that is why we do not do it more often. We add this information:

"One should keep in mind that our modelling approach neglects the change of the front during the period of interest between two observations of frontal positions (11 days for most cases)."

p.15 Tab.4: "modelled" $\rightarrow$ ***"estimated": the melt is estimated from observations, not modeled. What is*** $\dot{a}_m^o bs$ ***? Also add zero values where appropriate instead of leaving empty spaces.***

This was a mistake, this should be $\dot{a}_m$.

p.16 Fig.9: $\dot{a}_c = \dot{a}_{c,u} - \dot{a}_{c,L}$ ***on p.15 (minus not plus), so it's not clear what is shown on this figure.***

$\dot{a}_{c,L}$ is actually negative so what is shown on the figure is $-\dot{a}_{c,L}$. We change the figure accordingly.

p.19 l.5: "Due to this, there is some uncertainty" → "There is therefore some uncertainty"

Done!

p.19 l.7: Add references (or something else) to justify this statement that is not supported.

We have rewritten and added references to support this statement:

"Previous work has suggested that intra-annual changes in the ambient stratification are small enough that plumes are relatively insensitive to these changes (Slater et al., 2017) and that plume models forced with variations in runoff and a constant ambient stratification can qualitatively reproduce observations (Stevens et al., 2016)."

p.19 l.24: Is that what is observed by the authors?

Yes.

p.20 l.1: "no retreat at all": this is not supported by the model results, there is some retreat in the southern part of the domain.

We meant no retreat at all at SD. We add this information.

p.20 l.9-10: I don't think that the experiments made and results support such a conclusion, the role of sliding and geometry cannot be clearly separated.

See answer to major comment and new rewriting of the section.

p.20 l.19: "the velocity higher" → "the higher velocity"

Done!

p.20 l.19: "seem" → "seems"

Done!

p.20 l.30: "reproduces" → "reproduced"

Done!

p.21 l.12: "in 2D" → "with a simplified 2D geometry"

Done!

p.21 l.14: How do the melt rates compare to previous results?

There are no previously published frontal melt rates for this glacier (modelled or observed), so no comparison is possible.

p.21 l.23: What is referred to as the calving model?

We mean the discrete particle model. The text has been changed to make this clear.

p.22 l.5: "would be implemented" → "were implemented"

Done!

References

Benn, D. I., Åström, J., Zwinger, T., Todd, J., Nick, F. M., Cook, S., Hulton, N. R., and Luckman, A.: Melt-under-cutting and buoyancy-driven calving from tidewater glaciers: new insights from discrete element and continuum model simulations, Journal of Glaciology, pp. 1–12, doi:10.1017/jog.2017.41, 2017.

Carroll, D., Sutherland, D. A., Shroyer, E. L., Nash, J. D., Catania, G. A., and Stearns, L. A.:

Modeling turbulent subglacial meltwater plumes: Implications for fjord-scale buoyancy-driven circulation, Journal of Physical Oceanography, 45, 2169–2185, doi:10.1175/JPO-D-15-0033.1, 2015.

Cottier, F., Tverberg, V., Inall, M., Svendsen, H., Nilsen, F., and Griffiths, C.: Water mass modification in an Arctic fjord through cross-shelf exchange: The seasonal hydrography of Kongsfjorden, Svalbard, Journal of Geophysical Research: Oceans, 110, doi:10.1029/2004JC002757, 2005.

Gagliardini, O., Zwinger, T., Gillet-Chaulet, F., Durand, G., Favier, L., de Fleurian, B., Greve, R., Malinen, M., Martín, C., Råback, P., Ruokolainen, J., Sacchettini, M., Schäfer, M., Seddik, H., and Thies, J.: Capabilities and performance of Elmer/Ice, a new-generation ice sheet model, Geoscientific Model Development, 6, 1299–1318, doi:10.5194/gmd-6-1299-2013, 2013.

Gillet-Chaulet, F., Gagliardini, O., Seddik, H., Nodet, M., Durand, G., Ritz, C., Zwinger, T., Greve, R., and Vaughan, D. G.: Greenland ice sheet contribution to sea-level rise from a new-generation ice-sheet model, Cryosphere, 6, 1561–1576, 2012.

Goldberg, D. N. and Sergienko, O. V.: Data assimilation using a hybrid ice flow model, The Cryosphere, 5, 315–327, 2011.

Holland, D. M., Thomas, R. H., De Young, B., Ribergaard, M. H., and Lyberth, B.: Acceleration of Jakobshavn Isbrae triggered by warm subsurface ocean waters, Nature geoscience, 1, 659–664, doi:10.1038/ngeo316, 2008a.

Holland, P. R., Jenkins, A., and Holland, D. M.: The response of ice shelf basal melting to variations in ocean temperature, Journal of Climate, 21, 2558–2572, doi:10.1175/2007JCLI1909.1, 2008b.

Jenkins, A.: Convection-driven melting near the grounding lines of ice shelves and tidewater glaciers, Journal of Physical Oceanography, 41, 2279–2294, doi:10.1175/JPO-D-11-03.1, 2011.

Luckman, A., Benn, D. I., Cottier, F., Bevan, S., Nilsen, F., and Inall, M.: Calving rates at tidewater glaciers vary strongly with ocean temperature, Nature communications, 6, doi:10.1038/ncomms9566, 2015.

Morlighem, M., Rignot, E., Seroussi, H., Larour, E., Ben Dhia, H., and Aubry, D.: Spatial patterns of basal drag inferred using control methods from a full-Stokes and simpler models for Pine Island Glacier, West Antarctica, Geophysical Research Letters, 37, 2010.

Slater, D., Nienow, P., Sole, A., Cowton, T., Mottram, R., Langen, P., and Mair, D.: Spatially distributed runoff at the grounding line of a large Greenlandic tidewater glacier inferred from

plume modelling, Journal of Glaciology, 63, 309–323, doi:10.1017/jog.2016.139, 2017.
Slater, D. A., Goldberg, D. N., Nienow, P. W., and Cowton, T. R.: Scalings for submarine melting at tidewater glaciers from buoyant plume theory, Journal of Physical Oceanography, 46, 1839–1855, doi:10.1175/JPO-D-15-0132.1, 2016.
Stevens, L. A., Straneo, F., Das, S. B., Plueddemann, A. J., Kukulya, A. L., and Morlighem, M.: Linking glacially modified waters to catchment-scale subglacial discharge using autonomous underwater vehicle observations, The Cryosphere, 10, 417–432, doi:10.5194/tc-10-417-2016, 2016.
Vallot, D., Pettersson, R., Luckman, A., Benn, D. I., Zwinger, T., Van Pelt, W., Kohler, J., Schäfer, M., Claremar, B., and Hulton, N. R. J.: Basal dynamics of Kronebreen, a fast-flowing tidewater glacier in Svalbard: local spatio-temporal response to water input, Journal of Glaciology (in press), 2017.
Xu, Y., Rignot, E., Fenty, I., Menemenlis, D., and Flexas, M. M.: Subaqueous melting of Store Glacier, west Greenland from three-dimensional, high-resolution numerical modeling and ocean observations, Geophysical Research Letters, 40, 4648–4653, doi:10.1002/grl.50825, 2013.

Interactive comment on The Cryosphere Discuss., https://doi.org/10.5194/tc-2017-166, 2017.

Printer-friendly version

Discussion paper

Effects of undercutting and sliding on calving: a ~~coupled~~ global approach applied to Kronebreen, Svalbard

Dorothée Vallot[1], Jan Åström[2], Thomas Zwinger[2], Rickard Pettersson[1], Alistair Everett[3], Douglas I. Benn[4], Adrian Luckman[5], Ward J. J. van Pelt[1], Faezeh Nick[6], and Jack Kohler[3]

[1]Department of Earth Sciences, Uppsala University, Sweden
[2]CSC - IT Center for Science, Espoo, Finland
[3]Norwegian Polar Institute, Fram Centre, N-9296 Tromsø, Norway
[4]School of Geography and Geosciences, University St Andrews, Scotland
[5]Swansea University, Wales, UK
[6]Arctic Geology Department, University Centre in Svalbard, Norway

Correspondence to: Dorothée Vallot

Abstract.

In this paper, we study the effects of basal friction, sub-aqueous undercutting and glacier geometry on the calving process ~~with~~ by combining six different models: a continuum-mechanical ice flow model (Elmer/Ice), a climatic mass balance model, a simple subglacial hydrology model, a plume model, an undercut model and a discrete particle model to investigate fracture dynamics (Helsinki Discrete Element Model, HiDEM). We ~~also~~ demonstrate the feasibility of reproducing the observed calving retreat at the front of Kronebreen, a tidewater glacier in Svalbard, during a melt season. Basal sliding and glacier motion ~~is~~ are addressed using Elmer/Ice while calving is modelled by HiDEM. ~~An~~ A hydrology model calculates subglacial drainage paths and indicates two main outlets ~~at relatively different rates~~with different discharge. Depending on the discharge, the plume model computes frontal melt rates, which are iteratively projected to the actual front of the glacier at subglacial discharge locations. This produces undercutting of different sizes, as melt is concentrated close to the surface for high discharge and is more diffuse for low discharge. By testing different configurations, we show that ~~the geometry (frontal position and topography) controls the calving location while basal sliding controls the calving rate. Undercutting~~ undercutting plays a key role in glacier retreat and is necessary to reproduce observed retreat in the vicinity of the discharge ~~location.~~ locations during the melting season. Calving rates are also influenced by basal friction, through its effects on near-terminus strain rates and ice velocity.

1 Introduction

Accelerated discharge of ice into the oceans from land ice is a major contributor to sea level rise, and constitutes the largest source of uncertainty in sea-level predictions for the twenty-first century and beyond (Church et al., 2013). To a large degree, this uncertainty reflects the ~~lack of rigorous methods of predicting ice losses by~~ limited understanding of processes impacting calving from tidewater glaciers and ice shelves, and associated feedbacks with glacier dynamics. In particular, calving occurs by the propagation of fractures, which are not explicitly represented in the continuum models used to simulate ice flow and glacier evolution.

Recently, it has been suggested that ocean warming could play an important role in determining glacier calving rate and acceleration, by impacting ~~on~~ submarine melt rates (Holland et al., 2008a; Luckman et al., 2015). ~~Straneo and Heimbach (2013)~~ Straneo and Heimbach (2013) proposed two mechanisms responsible for the increase of submarine melt rates at the ice-ocean interface in Greenland: a warmer and thicker layer of Atlantic water in the fjords and an increase in subglacial discharge mainly during ~~the summer and the~~ summer and autumn. Buoyant meltwater plumes entrain warm ocean water (Jenkins, 2011) and are thought to enhance melt undercutting (Slater et al., 2015) at the ice cliff ~~followed by ice-front collapse~~ triggering collapse of the ice above. Luckman et al. (2015) investigated controls on seasonal variations in calving rates and showed that calving variations at Kronebreen, the glacier this study focuses on, are ~~best~~ strongly correlated with sub-surface ocean temperature changes linked to melt undercutting of the calving front. However, direct measurements of oceanic properties, ice dynamics, frontal geometries and mean volumetric frontal ablation rates are still too scarce to quantify the relationship between ocean processes, subglacial discharge and ice dynamics and one must rely on modelling. Complex coupled process models can help to gain a better understanding of the physics taking place at ~~tide-water~~ tidewater glacier fronts.

In previous modelling work (Van der Veen, 2002; Benn et al., 2007; Amundson and Truffer, 2010; Nick et al., 2010; Cook et al., 2012; Krug et al., 2014, 2015), the dynamics of ice masses have been simulated using continuum models, in which the continuum space is ~~discretized~~ discretised and include processes of mass and energy balance. ~~Continuum~~ In addition to the lack of process understanding, continuum models cannot explicitly model fracture~~and calving processes~~, but must use simple parameterisations such as damage variables or phenomenological calving criteria. ~~These are largely untested against observations, and may fail to adequately represent key processes. These~~ These problems can be circumvented using discrete particle models, which represent ice as assemblages of particles linked by breakable elastic bonds. ~~Åström et al. (2013, 2014)~~ Ice is considered as a granular material and each particle obeys Newton's equations of motion. Above a certain stress threshold, the bond is broken, which allows the ice to fracture. Åström et al. (2013, 2014) showed that complex crevasse patterns and calving processes observed in nature can be modelled using a particle model, the Helsinki Discrete Element Model (HiDEM). ~~By~~ Bassis and Jacobs (2013) used a similar particle model and suggested that glacier geometry provides the first-order control on calving regime. However, the drawback of these models is that due to their high computer resource demand, they only can be applied to a few minutes of physical time. A compromise should be found by coupling a continuum model, such as Elmer/Ice, to a discrete model, ~~HiDEM, we aim to~~ such as HiDEM, to successively describe the ice ~~successively~~ as a fluid and as a brittle solid. Sliding velocities and ice geometry calculated with the fluid dynamic model are used by the discrete particle model to compute a new calving front position. The effect of subglacial drainage mixing with the ocean during the melt season is taken into account by using a plume model that estimates melt rates at the front according to pro-glacial observed ocean temperatures, subglacial discharge derived from surface runoff and ice front height.

In this paper, we ~~introduce the coupling~~ use both the capabilities of the continuum model Elmer/Ice ~~with the~~ and the discrete element model HiDEM. We ~~thus~~ harness the ability of HiDEM to model fracture and calving events, while retaining the long-term ice flow solutions of a continuum approach. The aim is to investigate the influence of basal sliding, geometry and undercutting at the calving front on calving rate and location. We determine the undercut with a high resolution plume model calculating melt rates from subglacial discharge. The simple hydrology model that calculates the subglacial discharge, is based

on surface runoff that is assumed to be transferred directly to the bed and routed along the surface of calculated hydrological potential. We illustrate the approach using data from Kronebreen, a fast-flowing outlet glacier in western Spitsbergen, Svalbard (topography, meteorological and oceanographic data, as well as horizontal surface velocity and front positions from 2013) to assess the feasibility of modelling calving front retreat (rate and position).

2 Study area

Kronebreen is a tidewater glacier~~situated close to the research station Ny-Ålesund~~ , that flows into Kongsfjorden in Svalbard, one of the fastest glaciers in the archipelago. The glacier front position undergoes seasonal oscillations, showing advance during the winter and spring followed by retreat in the summer and autumn. Since 2011, the summer retreat has outpaced the winter advance, with an overall net retreat of $\sim$2 km between 2011 and 2015 after a relatively stable period since the 1990s (Schellenberger et al., 2015; Luckman et al., 2015; Köhler et al., 2016). Velocities at the front can reach 5 $\mathrm{m\,d^{-1}}$ in the summer with large seasonal and annual variations associated with basal sliding (Vallot et al., 2017). In 2013, averaged velocities close to the front ranged from 2.2 to 3.8 $\mathrm{m\,d^{-1}}$ in the summer and fell to 2 $\mathrm{m\,d^{-1}}$ directly after the melt season. In 2014, however, they stayed relatively high (around 4 $\mathrm{m\,d^{-1}}$) throughout the summer and progressively fell to 3 $\mathrm{m\,d^{-1}}$ in the winter.

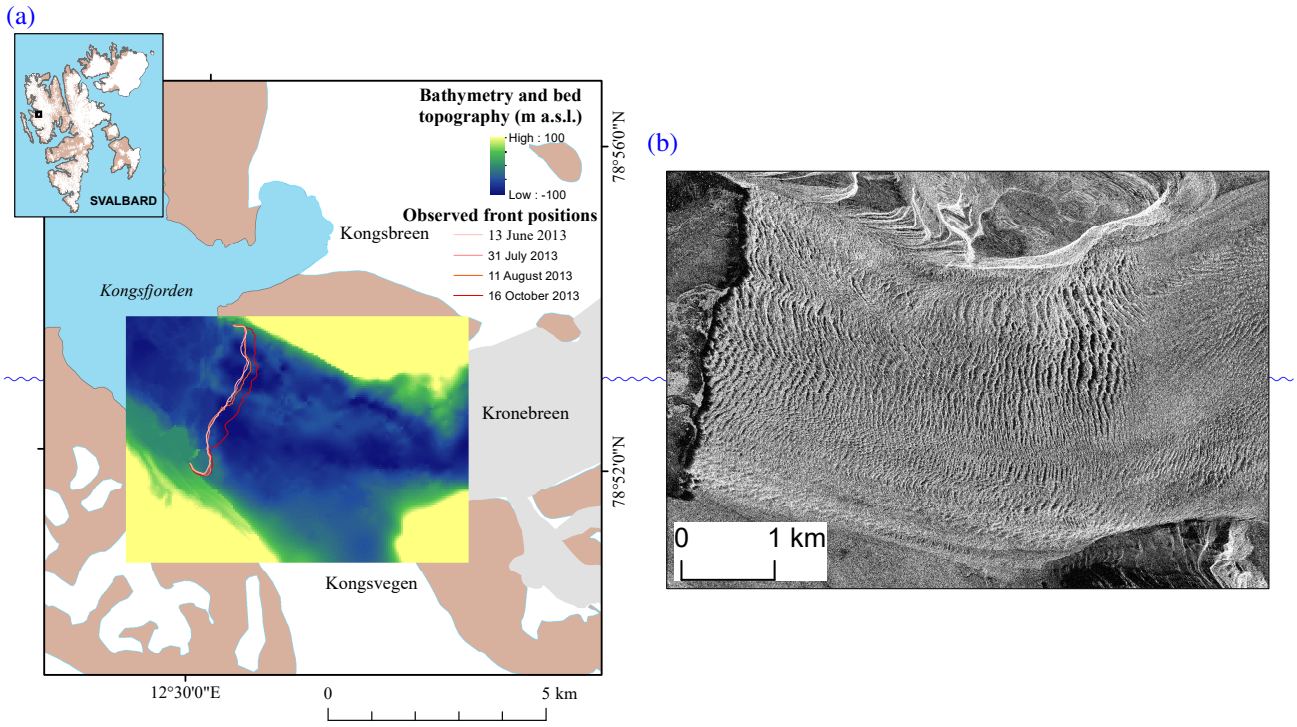

Figure 1. **(a)** Map of Kronebreen and its surrounding area. Ocean is in blue, bare rock is in red and glacier ice is in white. The grey area represents the Kronebreen glacier system. The inset map top left shows the location of Kronebreen in Svalbard ~~with four frontal position of interest. Bathymetry~~ , and the central inset panel shows fjord bathymetry and bed topography ~~are~~ in m a.s.l., and four frontal positions during 2013. **(b)** Crevasse pattern at the front of Kronebreen in August 2014 from TerraSAR-X satellite (1 m resolution).

~~The terminus of Kronebreen flows into Kongsfjorden and is characterised by plumes of~~ Plumes of turbid meltwater, fed by subglacial discharge, ~~that have been observed along the~~ are observed adjacent to the glacier terminus during the ~~melting~~ melt season (Trusel et al., 2010; Kehrl et al., 2011; Darlington, 2015; How et al., 2017). There are two main discharge points and the northern plume is generally more active than the southern one. Sediment-rich fresh meltwater discharge is thus mixing with saline fjord waters and can lead to a significant melt rate at the front of the glacier. Large variations of marine processes are typical for arctic fjords and Kongsfjorden ~~seems to experience~~ experiences significant influx of warm water masses during the summer (Cottier et al., 2005) as shown by ~~(Nahrgang et al., 2014) presenting~~ observations presented by Nahrgang et al. (2014) of ocean temperatures of Kongsfjorden from moored observatories in 2012-2013. From October to mid-November 2012, the whole water column temperature ~~is~~ was warm (4-5 °C). Thereafter, the upper 100 m ~~become~~ became colder and in January 2013, the whole water column temperature ~~drops~~ dropped to 1-3 °C. From March to May, it ~~approaches~~ approached 0 °C and ~~starts~~ started to increase again in May (1-3 °C). In August, the temperature ~~has~~ had reached 3-4 °C and the upper 100 m ~~increase~~ increased particularly to reach 5-6 °C towards the end of the season. Fjord bathymetry (Howe et al., 2003; Aliani et al., 2016) and bed topography under the glacier systems ~~have been collected by (Lindbäck et al., 2017) and~~ (Lindbäck et al., 2017) reveal a glacier terminus ~~height~~ thickness of about 150 m at the discharge locations with 100 m of submerged column (see Fig. 1).

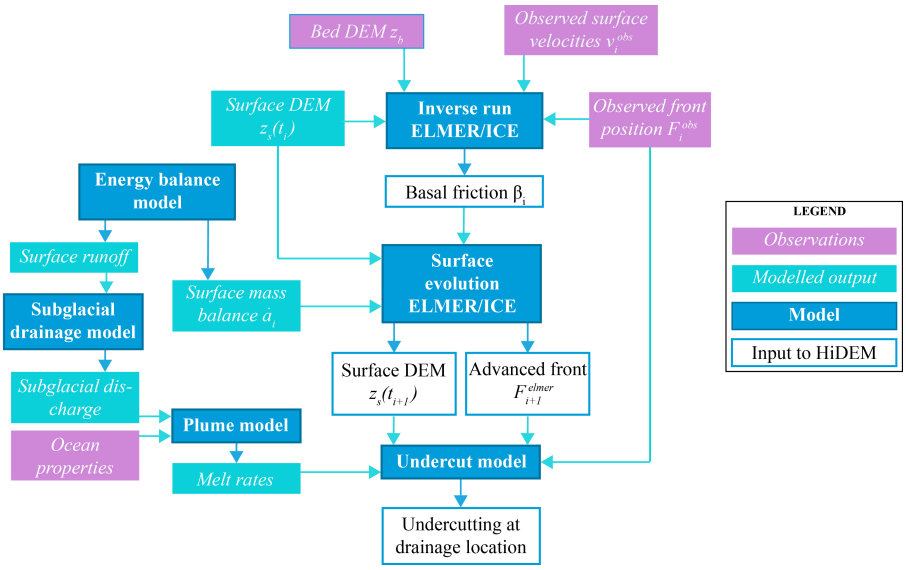

Figure 2. Model scheme presenting the calculation of the sliding and geometry (Elmer/Ice) as well as the undercutting at the subglacial discharge as input to the glacier calving from the HiDEM.

Close to the subglacial discharge locations, a changing grounding-line fan of sediments has been observed (Trusel et al., 2010) potentially ensuring a pinning point if the glacier were to advance in the future. Luckman et al. (2015) showed that calving rates are strongly correlated with subsurface fjord temperatures, indicating that the dominant control on calving is melt undercutting, followed by collapse of the sub-aerial part.

3 Methods

3.1 Observed geometry, surface velocities and front positions

The bed topography, z_b, is derived from profiles of airborne and ground-based common-offset ice penetrating radar surveys distributed over Kronebreen from 2009, 2010 and 2014 (Lindbäck et al., 2017). The initial surface topography includes different available surface DEMs and is described in Vallot et al. (2017).

Ice surface velocities were derived from feature tracking of TerraSAR-X image pairs in slant range using correlation windows of 200×200 pixels at every 20 pixels, and subsequently ortho-rectified to a pixel size of 40 m using a digital elevation model (Luckman et al., 2015). ~~Acquisition is done~~ Images were acquired roughly every 11 days for the period May-October 2013. Uncertainties in surface velocity are estimated to be $\sim 0.4\,\mathrm{m\,d^{-1}}$, and comprise a co-registration error ($\pm$ 0.2 pixels) and errors arising from unavoidable smoothing of the velocity field over the feature-tracking window. Ice-front positions were manually digitised from the same images used for feature tracking after they had been orthorectified to a pixel size of ~~2m~~ 2 m using a surface DEM ~~Luckman et al. (2015)~~(Luckman et al., 2015).

3.2 One-way coupling approach

We use surface velocity and frontal position data described above to test the effects of sliding and undercutting on calving ~~by coupling different models~~ using different models in a global approach. This one-way coupling approach is divided into three parts using six models (see Fig. 2): computing sliding and geometry (with Elmer/Ice), determining ~~of~~ undercutting (with the energy balance model, subglacial hydrology model, plume model and undercutting model) and computing calving (with HiDEM). ~~We first infer sliding from surface velocities using an adjoint inverse method implemented in Elmer/Ice with an updated geometry from observations at different time steps.~~

Table 1. Time step and associated date.

~~Time step~~ t_i	Δt_i	Date	Comment
t_0		2 June 2013	Before the onset of the melting season
t_1	11 d	13 June 2013	First melt
t_2	11 d	24 June 2013	
t_3	11 d	5 July 2013	
t_4	26 d	31 July 2013	Period of high surface runoff
t_5	11 ~~August~~ d	11 Aug. 2013	
t_6	11 d	22 Aug. 2013	Minimum basal friction
t_7	11 d	2 ~~September~~ Sept. 2013	
t_8	11 d	13 ~~September~~ Sept. 2013	
t_9	11 d	24 ~~September~~ Sept. 2013	
t_{10}	11 d	5 ~~October~~ Oct. 2013	
t_{11}	11 d	16 ~~October~~ Oct. 2013	After the last melt

We set t_0 at the velocity acquisition just before the first melt and the following time steps are set at each observation of surface velocity. The exact dates are summarized in Table 1.

First, we infer sliding at each time step from surface velocities using an adjoint inverse method implemented in Elmer/Ice with an updated geometry from observations at different time steps. At each iteration, i, corresponding to an observed front position, F_i^{obs}, the front and the surface are dynamically ~~evolving to the next front position observation time iteration~~ evolved during the observation time (roughly 11 days) ~~.~~ with Elmer/Ice. By the end of the time step, the front has advanced to a new position, F_{i+1}^{elmer}. Here we use $i+1$ because this is the position the front would have at t_{i+1} in the absence of calving. Second, given subglacial drainage inferred from modelled surface runoff, a plume model calculates melt rates based on the subglacial

discharge for each iteration, which are subsequently applied to the front geometry at subglacial discharge locations. At each iteration, the front geometry takes into account the undercut modelled at the former iteration. Finally, the sliding, geometry and undercut (when applicable) are taken as input to the calving particle model HiDEM for each iteration ~~,~~ and a new front, F_{i+1}^{hidem}, is computed for four iterations, t_0, t_4, t_6, t_{11}, which represent interesting cases (see comments on Table 1). More details about each aspect of the model process are given in the following sections.

We call this approach a one-way coupling because inputs to the HiDEM are output results from Elmer/Ice and undercutting model but not vice versa. In Elmer/Ice, we use the observed frontal positions. A completely coupled physical model would use the output of the HiDEM, the modelled front position, as input to the ice flow model Elmer/Ice and the undercutting model. It would also calculate the basal friction from a sliding law rather than an inversion. ~~We therefore chose to first study the effect of sliding before performing a full coupling.~~ In principle, such an implementation is possible using the same ~~steps~~ model components as this study.

3.3 Sliding and frontal advance with continuum model Elmer/Ice

At the base of the glacier, we use a linear relation for sliding ~~law~~ of the form

$$\tau_{\mathbf{b}} + \beta \underline{u} \mathbf{v_b} = \mathbf{0}, \tag{1}$$

with ~~τ_b~~ $\tau_{\mathbf{b}}$, the basal shear stress and ~~u_b~~ $\mathbf{v_b}$, the basal velocity. The basal friction coefficient, β, is optimized at each time step to best reproduce observed velocity distribution at the surface of the glacier ~~(Vallot et al., 2017). That~~ as described in Vallot et al. (2017). This is done by using ~~the self-adjointness~~ a self-adjoint algorithm of the Stokes equations for an inversion (e.g. Morlighem et al., 2010; Goldberg and Sergienko, 2011; Gillet-Chaulet et al., 2012) and implemented in Elmer/Ice (Gagliardini et al., 2013). The inversion is performed using the method of Lagrange multipliers to minimise a cost function including the observed horizontal surface velocities and a Tikhonov regularisation~~(Vallot et al., 2017).~~. We use an unstructured mesh, with spatial repartition of elements based on the mean observed surface velocities in the horizontal plane (roughly 30 m resolution close to the front). Vertically, the 2D mesh is extruded with ten levels (roughly 10 m resolution close to the front). More details on the model (viscosity, ice temperature, inversion time-steps, etc.) are given in Vallot et al. (2017).

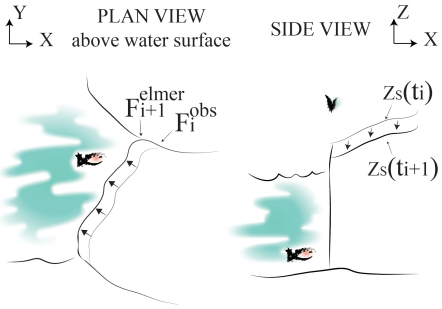

Figure 3. Front position and surface elevation changes with Elmer/Ice during $\Delta t = t_{i+1} - t_i$.

~~The bed topography, z_b, is derived from profiles of airborne and ground-based common-offset ice penetrating radar surveys distributed over Kronebreen (Lindbäck et al., 2017). The initial surface topography includes different available surface DEMs.~~ After each inversion, the temporal evolution of the glacier is mathematically described by the kinematic boundary condition defined at the surface,

$$\frac{\partial z_s}{\partial t} + u_x(z_s)\frac{\partial z_s}{\partial x} + u_y(z_s)\frac{\partial z_s}{\partial y} - u - v_z(z_s) = \dot{a}_s(t_i), \tag{2}$$

which describes the evolution of the free surface elevation, $z = z_s$, in reaction to a given net accumulation, $\dot{a}_s(t_i)$, calculated using a coupled modelling approach after Van Pelt and Kohler (2015), described in the next section. We use a time step of 1 day.

~~The front position is also able to advance and we~~ We assume that the front is vertical above the sea level so that the observed front position (at the surface of the glacier) is the same at sea level. We will call $F_i^{obs}(z = 0)$, the front position observed at time t_i with $z = 0$ at the sea level and $F_{i+1}^{elmer}(z = 0)$, the advanced modelled front position after $\Delta t = t_{i+1} - t_i$ (see Fig. 3). The front is advanced by imposing a Lagrangian scheme over a distance equal to the ice velocity multiplied by the time step. We do not account for the melting during the advance because we only have observations at the beginning and the end of each timespan. Instead, we lump frontal melting by applying an undercut after the advance as explained hereafter.

3.4 Surface runoff and subglacial discharge model

The surface mass balance, $\dot{a}_s$, and runoff are simulated with a coupled energy ~~balance - snow~~ balance-snow modelling approach (Van Pelt and Kohler, 2015). The coupled model solves the surface energy balance to estimate the surface temperature and melt rates. The subsurface routine simulates density, temperature and water content changes in snow and firn while accounting for melt water percolation, refreezing and storage. The model is forced with 3-hourly meteorological time-series of temperature, precipitation, cloud cover and relative humidity from the Ny-Ålesund weather station (eKlima.no; Norwegian Meteorological Institute). Elevation lapse rates for temperature are calculated using output from the Weather Research and Forecast (WRF) model ~~Claremar et al. (2012)~~(Claremar et al., 2012), while the precipitation lapse rate is taken from ~~(Van Pelt and Kohler, 2015)~~Van Pelt and Kohler (2015); zero lapse rates are assumed for cloud cover and relative humidity. Surface runoff is modelled on a 100×100 grid.

The temporal subglacial discharge at the calving front is estimated from integration of daily surface runoff assumed to be directly transferred down to the glacier bed. Assuming the basal water pressure at over burden, the flow path of the melt-water towards the glacier front is determined from the hydraulic potential surface defined as

$$\phi = \rho_i g(z_s - z_b) + \rho_w g z_b, \tag{3}$$

with g, the gravitational acceleration. The grid is the same as that used for surface runoff. The flow path along the ~~bed~~ hydraulic potential surface is determined by D-infinity flow method where the flow direction from a grid cell is defined as the steepest triangular facets created from the 8-neighboring grid cells (Tarboton et al., 1987). The flow from the center grid cell is distributed proportionally to the two cells that define the steepest facet. The flow is accumulated as the melt water is routed along

the calculated hydraulic potential surface towards the front and outlet points at the front are determined by identifying flow rates higher than $1\,\mathrm{m^3\,s^{-1}}$. The hydraulic potential surface is filled before flow accumulation is calculated to avoid sinks.

3.5 Plume model and submarine melt rates

A high-resolution plume model is used here to simulate the behaviour of subglacial discharge at the terminus of Kronebreen. The model is based upon the fluid dynamics code Fluidity (Piggott et al., 2008) which solves the Navier-Stokes equations on a fully unstructured three-dimensional finite element mesh. The model formulation builds upon the work of Kimura et al. (2013), with the addition of a large eddy simulation (LES) turbulence model (Smagorinsky, 1963) and the use of the synthetic eddy method (SEM) at the inlet (Jarrin et al., 2006).

The geometry of the model is adapted to Kronebreen by setting the water depth to 100 m and initialising the model with ambient temperature and salinity profiles collected from ringed seals instrumented with GPS-equipped Conductivity, Temperature and Depth Satellite Relay Data Loggers (GPS-CTD-SRDLs) (Boehme et al., 2009; Everett et al., 2017). These data were collected between 14th August and 20th September 2012 from a region between one and five ~~kilometres~~ kilometers away from the glacier terminus and are taken as representative of the ambient conditions in the fjord during summer. Melt rates are calculated on the terminus using a three-equation melt parameterisation described by Jenkins and Bombosch (1995) and McPhee et al. (2008) and implemented in Fluidity by Kimura et al. (2013). Velocities driven by ocean circulation are typically around ~~2–3~~ 2–3 orders of magnitude smaller than plume velocities and therefore neglected.

The model is spun-up for 1000 model seconds until the turbulent kinetic energy in the region of the plume reaches a steady state and thereafter run for 10 minutes of steady-state model time. Melt rates are extracted from the duration of the steady-state period, then time averaged and interpolated onto a uniform $1\times1\,\mathrm{m^2}$ grid covering a 400-m-wide section of the glacier terminus.

The high-computational cost of the model means that it cannot be run continuously over the study period, nor can the full range of discharges and oceanographic properties be tested. Instead, representative cases M_d using ~~uniform~~ the ambient ocean properties described above and discharges d of 1, 10, 50 and $100\,\mathrm{m^3\,s^{-1}}$ were tested and the melt rate profiles for intermediate discharges were linearly interpolated from these cases.

3.6 Undercutting model

We assume a vertically aligned surface front at the beginning of the melt season. We know the position of the front, $F_0^{obs}(z=0)$, ~~at each passage of the satellite~~for the time span of each satellite image. The front is spatially digitized with 10 m spacing in the horizontal space and 1 m spacing in the vertical space. We use the combination of observed front, advanced front and melt rates to estimate the daily amount of undercutting. ~~Sea level is situated at $z=0$.~~

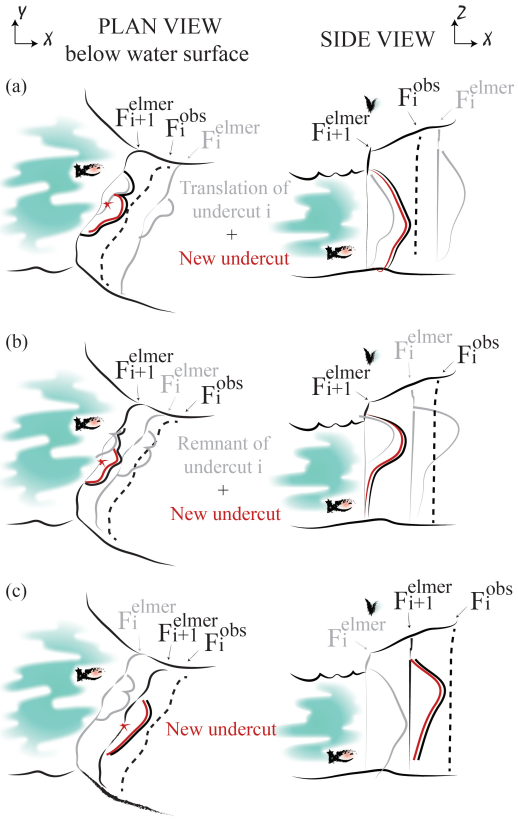

Figure 4. Three cases of former undercut position at z relative to $F_i^{obs}(z=0)$. The red star represents the discharge location. **(a)** $F_i^{obs}(z=0)$ is behind $F_{i+1}^{elmer}(z=0)$ and in front of $F_i^{elmer}(z)$. The undercut from $F_i^{elmer}(z)$ is translated to $F_{i+1}^{elmer}(z)$ (gray color) and the new undercut is superposed (red color). **(b)** $F_i^{obs}(z=0)$ is in front of $F_i^{elmer}(z)$. The remnant from $F_i^{elmer}(z)$ (what is behind $F_i^{obs}(z=0)$) is translated to $F_{i+1}^{elmer}(z)$ (gray color) and the new undercut is superposed (red color). **(c)** $F_i^{obs}(z=0)$ is behind $F_i^{elmer}(z)$. The undercut from $F_i^{elmer}(z)$ is ignored and the undercut created at t_{i+1} is the only one (red color).

When the first discharge occurs, the melt rate calculated with the plume model in 2D is summed for the period of time between t_0 and t_1 and projected to the advanced front $F_1^{elmer}(z=0)$ (advanced from $F_0^{obs}(z=0)$) at the location of the subglacial outlets and ice is removed normal to the front. This yields a new position of the front at depth z below sea level called $F_1^{elmer}(z)$. At the second iteration, t_2, we know where the front would be if there had not been any calving between t_1 and t_2: $F_2^{elmer}(z=0)$, which is the advanced front from the observed position at t_1, $F_1^{obs}(z=0)$. So we can transfer the whole undercut from previous iteration to $F_2^{elmer}(z)$ if $F_1^{obs}(z=0)$ is situated in front of $F_1^{elmer}(z)$ (see Fig. 4b–c). Otherwise, the undercut would have been fully or partly calved away (see Fig. 4b–c). We then apply the new undercut on this new geometry given the melt rates between t_1 and t_2.

At time t_i, the modelled front position at depth z (advanced by Elmer/Ice from the observed front position at t_{i-1}) is $F_i^{elmer}(z)$ and the observed front position is $F_i^{obs}(z=0)$. We advance this observed front with Elmer/Ice during $\Delta t = t_{i+1} - t_i$ to obtain the front position $F_{i+1}^{elmer}(z=0)$ at t_{i+1}. We want to determine $F_{i+1}^{elmer}(z)$ and depth z given the melt rate calculated

between t_i and t_{i+1} and the state of the undercut from the previous front $F_i^{elmer}(z)$ updated by the observed front $F_i^{obs}(z=0)$. Three different cases, depending on the relative position of the observed and modelled fronts at depth z, are then possible as shown in Fig. 4:

- if the new observed position $F_i^{obs}(z=0)$ is behind $F_i^{elmer}(z=0)$ and in front of $F_i^{elmer}(z)$, the melted undercut is kept and advances in the flow direction the same distance as the surface modelled front $F_{i+1}^{elmer}(z=0)$ (see Fig. 4a),
- if the new observed position $F_i^{obs}(z=0)$ is in front of $F_i^{elmer}(z)$, the undercut is displaced to the next modelled front $F_{i+1}^{elmer}(z=0)$ (see Fig. 4b),
- if the new observed position $F_i^{obs}(z=0)$ is behind $F_i^{elmer}(z)$, the front starts from a vertical profile again (see Fig. 4c).

The melt summed up between t_i and t_{i+1} is then applied to $F_i^{elmer}(z)$ to obtain $F_{i+1}^{elmer}(z)$ and so on. Melt above the surface has not been taken into account so that the effect of submerged ice feet ~~, regarded as a third order process by Benn et al. (2007) ,~~ is not described. The bed topography, the new geometry (surface elevation, front position with or without undercut) and the basal friction are then interpolated onto a 10×10 m grid to feed the HiDEM and a new front, F_{i+1}^{hidem} is modelled by calving.

3.7 Calving with first-principles ice fracture model HiDEM

The fracture dynamics model is described in detail in ~~Åström et al. (2014, 2013)~~Åström et al. (2014, 2013). This first-principles model is constructed by stacking blocks connected by elastic and breakable beams representing discrete volumes of ice. For computational efficiency, we use a block size of 10 m.

At the beginning of a fracture simulation, the ice has no internal stresses and contains a few randomly distributed broken beams~~with no internal stresses~~, representing small pre-existing cracks in the ice. The dynamics of the ice is computed using a discrete version of Newton's equation of motion, iteration of time steps and using inelastic potentials for the interactions of individual blocks and beams. As the ice deforms under its own weight, stresses on the beams increase, and if stress reaches a failure threshold the beam breaks and the ice blocks become disconnected but continue to interact as long as they are in contact. In this way cracks in the ice are formed. For computational reasons, we initialise the glacier using a dense packed face-centered cubic (fcc) lattice of spherical blocks of equal size. This introduces a weak directional bias in the elastic and fracture properties of the ice. The symmetry of the underlying fcc-lattice is however easily broken by the propagating cracks. The ground under the ice or at the sea-floor is assumed to be elastic with a linear friction law that varies spatially (Eq. 1).

The time step is limited by the travel time of sound waves through a single block and is thereby set to 10^{-4} ~~sec~~s. If the stress in the ice exceeds a fracture threshold, crevasses will form and ice may calve off the glacier. The duration of a typical calving event at Kronebreen is a few tens of seconds followed by a new semi-equilibrium when the ice comes to rest. The model run for ~100 s, which takes two days of simulation physical time. As HiDEM cannot be triggered too often because of computational limitations, we simulate ice flow with Elmer/Ice and compute calving with HiDEM thereafter. Calving events will then appear as fewer but bigger events compared to observations. If the time step is changed, the overall rate change stays roughly within $\pm 50\%$ (Benn et al., 2017).

The basal friction coefficients, β, at the front of Kronebreen are in the order of 10^8-$10^{12}\,\mathrm{kg\,m^{-2}\,s^{-1}}$ (Vallot et al., 2017) and to avoid instabilities to build up, a cut-off value, above which particles are assumed to be stuck to the bed substrate, is fixed at $\beta = 10^{12}\,\mathrm{kg\,m^{-2}\,s^{-1}}$.

HiDEM reads a file with surface and bed coordinates on a grid and a file with surface and basal ice (to take into account the undercut) coordinates. When simulating with an undercut at a discharge location and in order to avoid complication in the HiDEM (position of the basal ice), we remove particles below the maximum melt (no ice foot).

In the ocean, the basal friction coefficient is extrapolated downstream of the front and taken equal to the mean of the values at further from the terminus in case the ice advances. ~~Due to the very high bed friction, hardly any sliding motion would take place during the few minutes of a HiDEM simulation, which will affect the calving behaviour. Because of the different time scales of calvingand sliding processes, it is however possible to scale down the friction some orders of magnitude while still maintaining the separation of time-scales. Sliding is therefore scaled down to roughly correspond to a HiDEMsimulation physical time, which better represents the time-scale separating non-negligible calving events at Kronebreen.~~

~~An ice block is calved when all bounds are broken from the main piece of ice even though it does not separate from the~~ An ice block is calved when all bonds are broken from the glacier even though it does not separate from the front.

There is a clear separation of timescales between the velocities of sliding ($\sim\mathrm{m\,day^{-1}}$) and calving ice ($\sim\mathrm{m\,sec^{-1}}$). This means that as long as sliding is slow enough to be negligible during a single calving event, we can change it without much effect on any single calving event. As an approximation we can assume that fast processes are at equilibrium when we consider slower timescales. However, a rescaling speeds up the frequency of calving, and we can thus 'speed up', within reason, the few minutes of HiDEM simulation to effectively model calving which would otherwise take tens of hours or days, and thus be practically impossible to simulate with HiDEM. By applying scaling, the calving events modelled during the simulation of HiDEM (few minutes) correspond to the sum of calving events that would happen during the time scale of sliding. The scaling factor that we use is the same for the whole domain and for all simulations. We use a friction scaling factor for β equal to 10^{-2} (or sliding velocity scaled up by 10^2), and simulations run until calving stops and a new quasi-static equilibrium is reached.

In a fully coupled model, the altered ice geometry after calving could then be re-implemented in the flow model, acting as the initial state for a continued prognostic simulation with the continuum model. Here, this back-coupling is replaced by prescribing the next configuration obtained by satellite.

3.8 Frontal ablation calculation

The mean volumetric frontal ablation rate (or mean volumetric frontal calving rate) at the ice front at ~~the water margin at~~ time t_i, $\dot{a}_c(t_i)$, is the difference between the ice velocity at the front, ~~$u_w(t_i)$~~ $v_w(t_i)$ and the rate of change of the frontal position, $\partial L/\partial t$ integrated over the terminus domain ~~Γ_w~~ Σ_w as defined in McNabb et al. (2015). This yields

$$\dot{a}_c(t_i) = \int_{\Gamma_w} u_{\Sigma_w} v_w(t_i) - \frac{\partial L}{\partial t}\,\mathrm{d}\Gamma\Sigma_w, \tag{4}$$

with

$$\int_{\Gamma_w}\int_{\Sigma_w} \frac{\partial L}{\partial t}\,\mathrm{d}\Gamma\Sigma_w = \frac{\Delta A(t_i)}{t_i - t_{i-1}} \int_{z_{\Gamma_w}}\int_{z\in\Sigma_w} \mathrm{d}z \tag{5}$$

and $\Delta A(t_i)$, the area change at the terminus over the time $t_i - t_{i-1}$. We want to compare the ablation rates from F_i^{elmer} for observed and modelled cases. For the observed case, the mean volumetric ablation rate is calculated between the advanced front F_i^{elmer} and the observed front F_i^{obs}. For the modelled case, ~~the ablation rate is calculated between~~ during one simulation with HiDEM, several calving events are triggered. Volumetric calving rate is then inferred from the difference between the initial, F_i^{elmer} ~~and the modelled front~~, and final position, F_i^{hidem}, of the front, after calving has stopped. The total subaqueous melt rate, $\dot{a}_m$, at the front of the glacier is omitted in this balance.

3.9 Calving scenario simulations

We investigate the effect of three different ~~parameterisations~~ parameters on calving activity: the geometry~~(, g_i),~~ corresponding to the frontal position and topography, the sliding velocity mainly influenced by the basal friction parameter (β_i) and the undercut~~at subglacial discharge (, u_i) for four distinctive~~ , at the subglacial discharge locations for four distinct times $t_i = \{t_0, t_4, t_6, t_{11}\}$ (see Table 1). The different configurations are referred as $C(g_i, \beta_j, u_i)$~~with $i, j \in [0, 4, 6, 11]$~~. If $u_i = 0$, there is no undercut, hence a vertical ice front at the subglacial discharge location. At $t = 0$, the melt season has not started yet so there is no modelled undercut. At $t = 11$, the melt season is finished and there is no modelled undercut. If $j \neq i$, the geometry, g_i, is taken at t_i and the basal friction, β_j, at t_j to assess the roles of geometry and basal sliding. We investigate basal friction at t_0 and t_6 since the former has maximum friction and the latter minimum friction of the studied cases. The ~~configuration~~ configurations studied in this paper are summarised in Table 2.

Table 2. Different configurations, ~~C_k~~ C, characteristics and periods.

Configuration	Characteristics	Applied to
$C(g_i, \beta_i, 0)$	Geometry at t_i Sliding at t_i Vertical front	$i \in [0, 4, 6, 11]$
$C(g_i, \beta_i, u_i)$	Geometry at t_i Sliding at t_i Undercut at discharge	$i \in [4, 6]$
$C(g_i, \beta_j, 0)$	Geometry at t_i Sliding at t_j Vertical front	$(i, j) \in [(0, 6), (6, 0)]$

4 Results

4.1 Basal friction coefficients

The basal friction coefficient, β, for the four runs presented above, is shown in Fig. 5. At t_0, before the melt season, the basal friction is high and roughly homogeneous over the first kilometer. At t_4, when the surface runoff is the highest, the pattern is similar but with a large offset. The lowest friction is reached at t_6, particularly at the front and in the southern part of the glacier. The highest friction is reached at t_{11} a kilometer from the front. Close to the front position, however, the friction is still high.

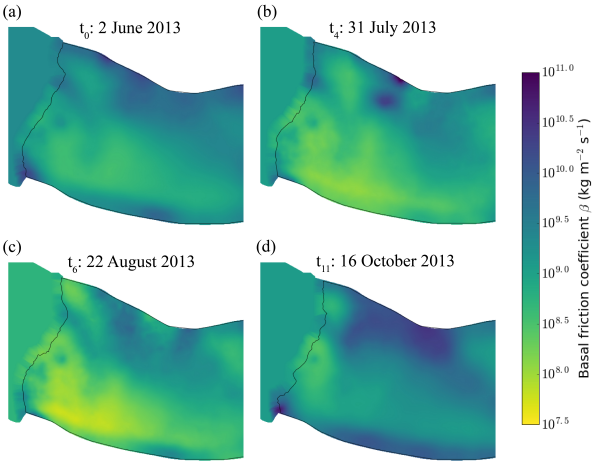

Figure 5. Basal friction coefficient and observed frontal position for **(a)** t_0: 2 June 2013, **(b)** t_4: 31 July 2013, **(c)** t_6: 22 August 2013 and , **(d)** t_{11}: 16 October 2013.

4.2 Subglacial discharge and submarine melt rates

The hydrological model predicts that there are two main subglacial channels ~~exceeding a discharge of~~ with discharge exceeding $1\,\mathrm{m}^3\,\mathrm{s}^{-1}$ of water (see Fig. 6a). This is in accordance with satellite and time-lapse camera images showing upwelling ~~(Trusel et al., 2010; Ke~~ ~~. Surface melt and consequently assumed~~ at these locations (Trusel et al., 2010; Kehrl et al., 2011; Darlington, 2015; How et al., 2017) . Modelled surface melt and discharge at the northern outlet - in short Northern Discharge (ND) - starts June 6 and ends October 1 while the discharge at the southern outlet (SD) starts June 21 and ends August 22. Fluxes at ND clearly exceed those at SD as shown in Fig. 6b and Table 3.

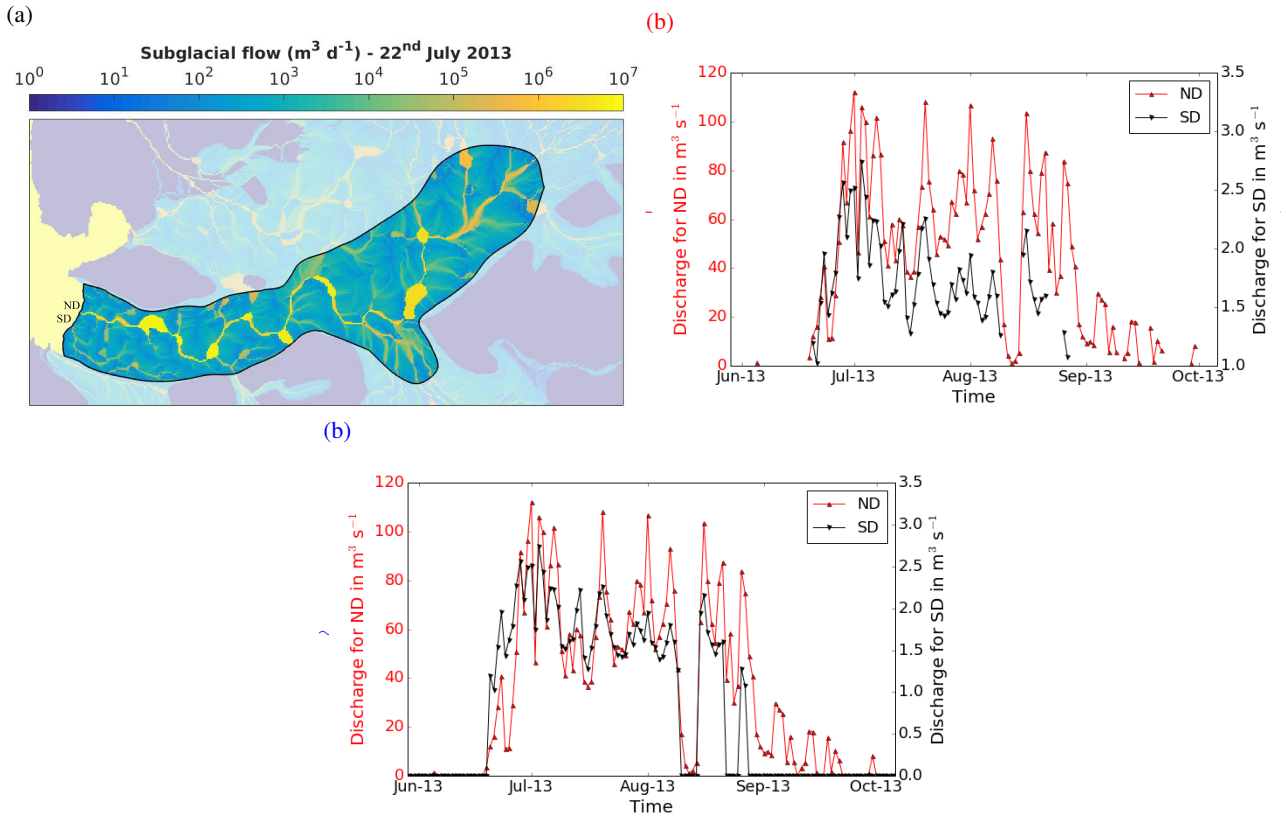

Figure 6. **(a)** Subglacial flow following the hydraulic potential surface (in $m^3\ d^{-1}$) in logarithmic scale on the 22nd July 2013. **(b)** Daily discharge for the northern and southern discharge (ND and SD respectively) during the melting season (data gaps ~~corresponds~~ correspond to no discharge).

Table 3. Total volume of subglacial discharge modelled per period of calving front recording.

Start date	End date	Days	Volume (m^3)	
			ND	SD
2 Jun (t_0)	13 Jun (t_1)	11	1.27e5	
13 Jun (t_1)	24 Jun (t_2)	11	8.73e6	4.94e5
24 Jun (t_2)	5 Jul (t_3)	11	6.24e7	2.05e6
5 Jul (t_3)	31 Jul (t_4)	26	1.10e8	3.54e6
31 Jul (t_4)	11 Aug (t_5)	11	6.2e7	1.36e6
11 Aug (t_5)	22 Aug (t_6)	11	4.69e7	1.04e6
22 Aug (t_6)	2 Sept (t_7)	11	3.91e7	2.03e5
2 Sept (t_7)	13 Sept (t_8)	11	1.18e7	0
13 Sept (t_8)	24 Sept (t_9)	11	6.20e6	0
24 Sept (t_9)	5 Oct (t_{10})	11	8.04e5	0
24 Sept (t_10)	5 Oct (t_{11})	11	0	0

The melt rate profiles calculated by the plume model for four different volumes of subglacial discharge are shown in Fig. 7.

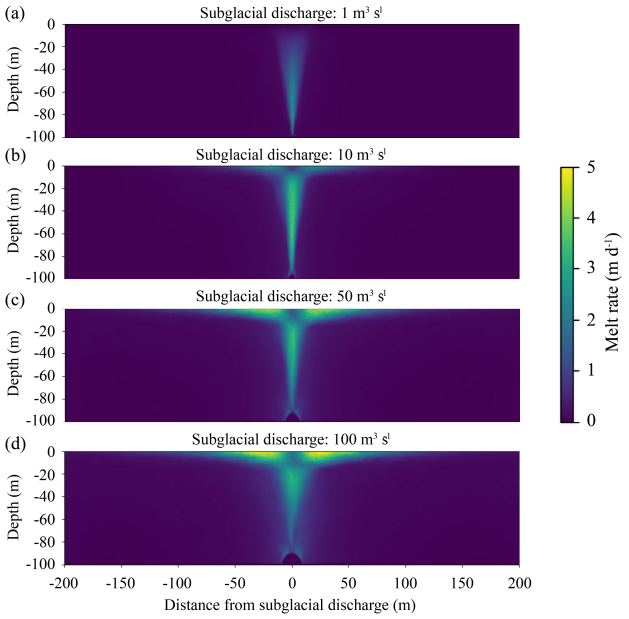

Figure 7. Melt rates, M_d, from the plume model given a discharge, d, of **(a)** $1\,\mathrm{m^3\,s^{-1}}$, **(b)** $10\,\mathrm{m^3\,s^{-1}}$, **(c)** $50\,\mathrm{m^3\,s^{-1}}$ and **(d)** $100\,\mathrm{m^3\,s^{-1}}$.

At a discharge of $1\,\mathrm{m^3\,s^{-1}}$, melt rates are low ($< 2.5\,\mathrm{m\,d^{-1}}$) with the maximum melt rate occurring at depth and negligible melt rates close to the water line. At $10\,\mathrm{m^3\,s^{-1}}$, the melt profile reaches the surface and has highest melt rates ($\sim 3.5\,\mathrm{m\,d^{-1}}$) along the plume column. With $50\,\mathrm{m^3\,s^{-1}}$ and $100\,\mathrm{m^3\,s^{-1}}$ discharge, the highest melt rates are attained at the ocean surface on the sides of the plume column ($\sim 5\,\mathrm{m\,d^{-1}}$ and $\sim 6\,\mathrm{m\,d^{-1}}$ respectively). In general, low discharges drive maximum melt within the plume and at depth, while higher discharges drive stronger surface gravity currents, and therefore gives higher melt rates at the surface.

4.3 Undercutting

The modelled frontal position is summarised in Fig. 8 in plan view and vertical view at the discharge locations. In most cases for the ND location, where the discharge is the highest, the melt profile (Fig. 8d) creates an undercut profile concentrated right near the waterline. Fried et al. (2015) found similar results when modelling melt rates at shallow grounding lines (~~100-250~~100–250 m) ~~plume model melt~~ given $250\,\mathrm{m^3\,s^{-1}}$ discharge. It is interesting to see that the observed front after calving, F_i^{obs}, (dashed line in Fig. 8a-b) generally falls behind the ~~undercutted~~ undercut front before calving, $F_i^{elmer}(z)$, (thick line in Fig. 8b).

The frontal submerged undercut driven by the plume differs in shape from one location to another. ~~The melting~~ In the first 50 m below the surface, the undercut at the SD is ~~smoother from the surface to approximately 50 m depth~~ not as abrupt as at the ND and is also ~~lower than ND~~ smaller (Fig. 8~~c-e). where~~ c–e). Where the discharge is the highest, the melt rate peaks just

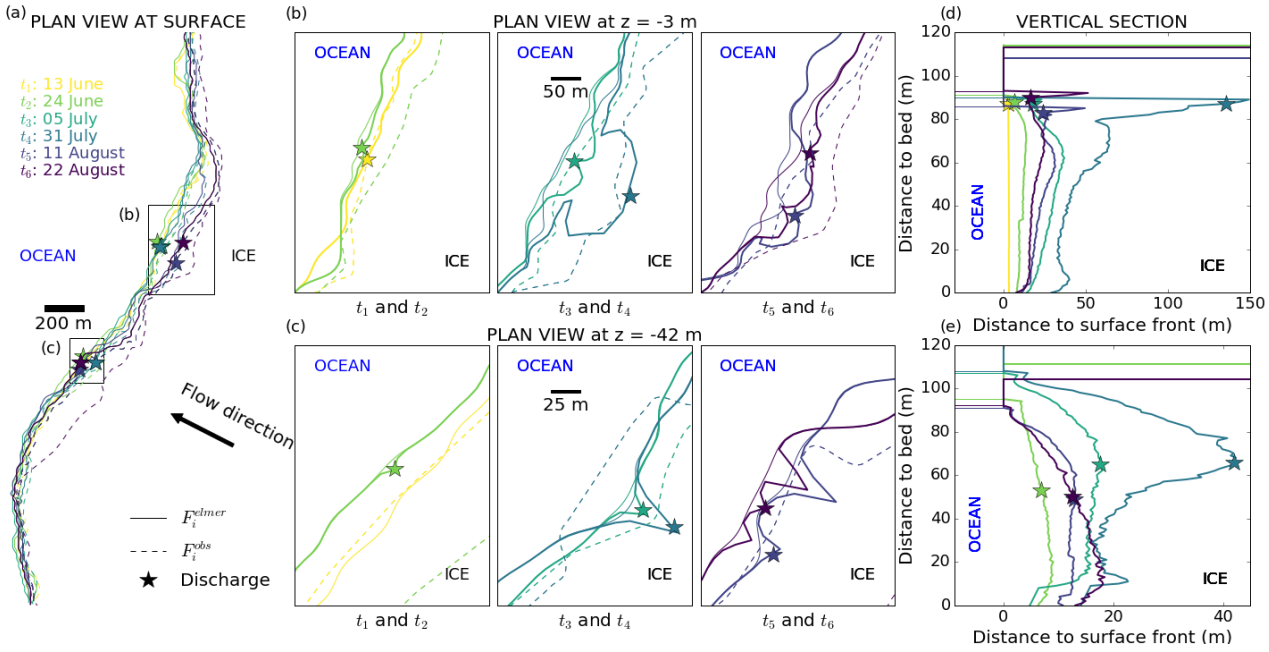

Figure 8. (a) Plan view of the frontal position of Kronebreen at six different dates, defined by different colors, corresponding to the satellite data acquisition dates during the ~~melting~~ melt season in 2013 (up to the 22nd of August). At t_i, the observed front, F_i^{obs}, is represented by a dashed line and the advanced front, $F_i^{elmer}(z=0)$, by a thin line. The discharge location is defined by a star. Enlargement at **(b)** the northern discharge (ND) area at $z=-3$ m and at **(c)** the southern discharge (SD) area at $z=-42$ m with the advanced front at depth z where undercut has been applied, $F_i^{elmer}(z)$, represented by a thick line. Vertical section **(d)** at the northern discharge (ND) location and at **(e)** the southern discharge (SD) location. The stars in (d,e) indicate the plan view elevation z from (b,c). Horizontal lines in **(d, e)** represent the sea level for each time step.

below the waterline and ~~stetching~~ stretches laterally from the vertical centerline of the plume~~but low~~. The lateral extent of melting is much lower at depth. At the SD, melting is strongest at depth due to lower discharge rates and less vigorous buoyant ascent of the plume. One should keep in mind that ~~this~~ our modelling approach neglects the change of the front during the period of interest between two observations of frontal positions (11 days for most cases). In reality, calving would occur more often during that period, making such large undercuts, as the modelled ones, not possible. This simplification has consequences for the next step when the particle model handles the calving of icebergs due to front imbalance.

4.4 Observed mean volumetric calving rates and modelled calving

The observed mean volumetric calving rate averaged over the entire calving front volume of ice, $\dot{a}_c^{obs}$ is the difference between the frontal velocity, ~~$u_w^{obs}(t_i)$~~$v_w^{obs}(t_i)$, and the rate of position change, $\partial L^{obs}/\partial t$ integrated over the terminus domain. These quantities and the total modelled ice mass melted by the plume normalised per day (when an undercut is prescribed) are given in Table 4.

Table 4. Observed mean volumetric calving rate, ~~$\dot{a}_c^{obs} = \dot{a}_{c,u}^{obs} - \dot{a}_{c,L}^{obs}$~~ $\dot{a}_c^{obs} = \dot{a}_{c,v}^{obs} - \dot{a}_{c,L}^{obs}$, in $10^5\ \mathrm{m^3\ d^{-1}}$, as the difference between the tangential (ice flow direction) ice velocity at the front and the rate of change of the frontal position integrated over the terminus domain, and ~~modelled~~ estimated subaqueous melt rate, $\dot{a}_m$, in $10^5\ \mathrm{m^3\ d^{-1}}$.

		$\mathbf{t_0}$	$\mathbf{t_4}$	$\mathbf{t_6}$	$\mathbf{t_{11}}$
$\dot{a}_c^{obs}$	~~$\dot{a}_{c,u}^{obs}$~~ $\dot{a}_{c,v}^{obs}$	2.63	3.68	4.31	2.56
	$\dot{a}_{c,L}^{obs}$	−5.30	−4.28	−22.63	−22.43
	Total	7.93	7.97	26.94	24.99
$\dot{\mathbf{a}}_\mathbf{m}$	**SD**	0	0.08	0.14	0
	ND	0	0.86	1.25	0
	Total	0	0.94	1.39	0
Ratio $\dot{\mathbf{a}}_\mathbf{m}/\dot{\mathbf{a}}_\mathbf{c}$		*0* %	*11.8* %	*5.2* %	*0* %

To assess the performance of the ~~pseudo-coupling~~one-way coupling, we evaluate the mean volumetric calving rate averaged over the entire calving front volume of ice (see Eq. 4), and the mean absolute distance between the modelled and the observed front, $|\bar{L}|$. These are presented in Fig. 9 for each configuration as well as the observed mean volumetric calving rate.

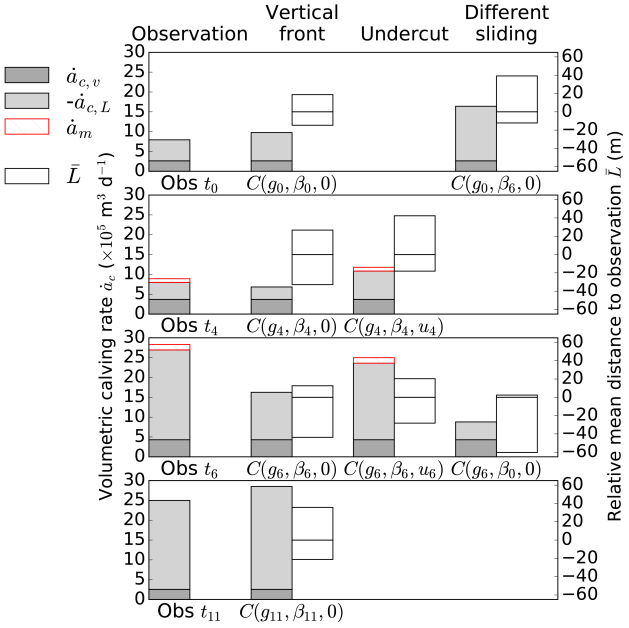

Figure 9. Observed and modelled mean volumetric calving ~~rate~~rates, $\dot{a}_c$, in $\mathrm{m^3\ d^{-1}}$ ~~is~~ are presented as the integrated tangential (ice flow direction) ice front velocity ~~$\dot{a}_{c,u}$~~ $\dot{a}_{c,v}$ (dark gray), the integrated rate of change of the frontal position, $\dot{a}_{c,L}$ (light gray) and the total subaqueous melt rate, $\dot{a}_m$ (hashed red) if an undercut is prescribed for each configuration. The mean distance ~~difference~~ differences between the modelled and the observed front positive and negative, ~~$|\bar{L}|$ is~~ $\bar{L}$ are shown on the right. A negative value corresponds to underprediction of calving position (modelled in ~~black~~front of observed).

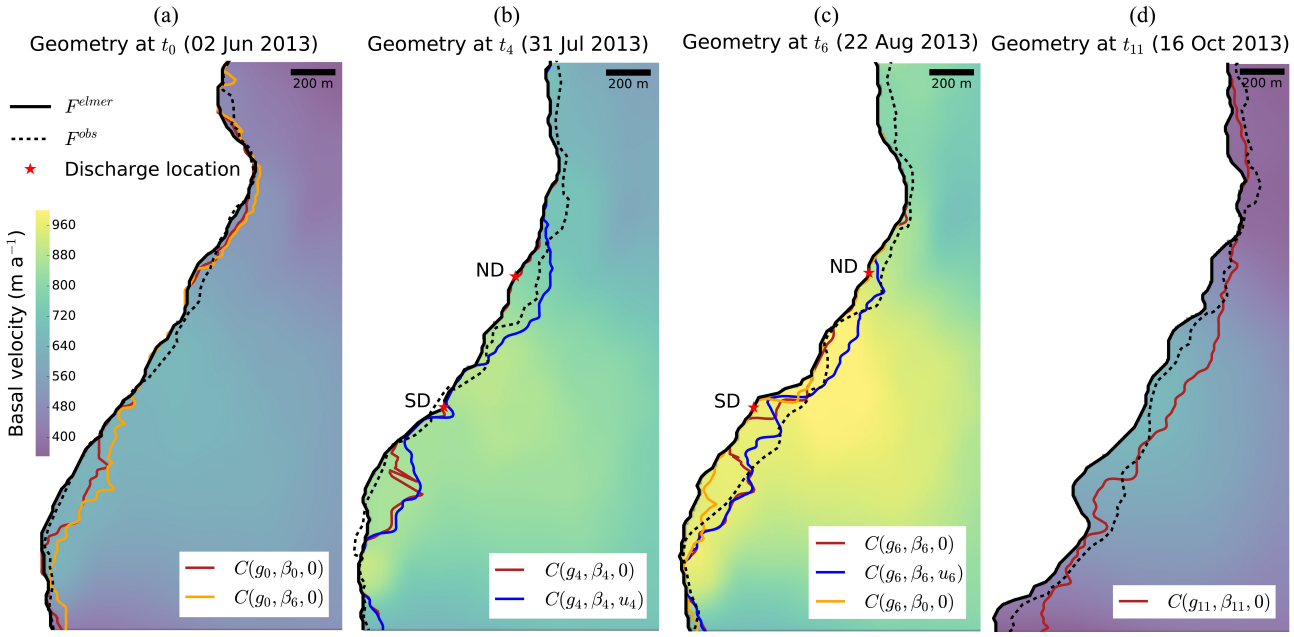

Figure 10. Basal velocity, advanced front before calving modelled with Elmer/Ice, F_i^{elmer}, at t_i in plain black, observed front after calving, F_i^{obs}, in dashed black and calving front modelled with HiDEM, F_i^{hidem} given the different configurations summarised in Table 2 for **(a)** $i = 0$, **(b)** $i = 4$, **(c)** $i = 6$, and **(d)** $i = 11$. Discharge locations (for $i = 4, 6$) are marked with a red star.

Fig. 10 shows the different front positions after the HiDEM simulation for each configuration of the studied time. Fig. 11 shows strain rates modelled by HiDEM that resemble a ~~crevasse pattern~~ observed crevasse patterns (yellow lines representing crevasses).

At t_0, before the melt started, the front has retreated at a rate of 7.93 $\times 10^5$ m^3 d^{-1} with a frontal ice flux of 2.63 $\times 10^5$ m^3 d^{-1}, mostly in the middle part with a calved area of 5.1×10^4 m^2. The HiDEM produces a slightly higher mean volumetric calving rate, 9.76 $\times 10^5$ m^3 d^{-1} with a vertical ice front configuration (red line $C(g_0, \beta_0, 0)$ in Fig. 10a) at a mean distance of 32 m from the observed front. However, calving is concentrated south of SD in a zone of high ice velocity and high strain rates as modelled by HiDEM (see Fig. 11).

With peak surface runoff, at t_4, the observed mean volumetric calving rate equals 7.97 $\times 10^5$ m^3 d^{-1}, similar to t_0 but with higher ice velocities (3.68 $\times 10^5$ m^3 d^{-1}). Observed retreat at ~~the ND location~~ and north of ~~it~~ ND is significant but is not reproduced by the configuration with a vertical ice front (red line $C(g_4, \beta_4, 0)$ in Fig. 10b). Instead the front is retreating south of SD in the same fashion as for t_0. The mean volumetric calving rate (6.82 $\times 10^5$ m^3 d^{-1}) is therefore close to the observed value, but the mean distance between the observed and the modelled front is close to 60 m (see Fig. 9). For the undercut configuration (blue line $C(g_4, \beta_4, u_4)$ in Fig. 10b), the mean volumetric calving rate is also overestimated at the same location but the observed retreat around ND is matched by the HiDEM. The mass removed by undercutting represents 11.8 % of the total observed mean volumetric calving rate (see Table 4) and is therefore non-negligible. At the SD, the observed front is

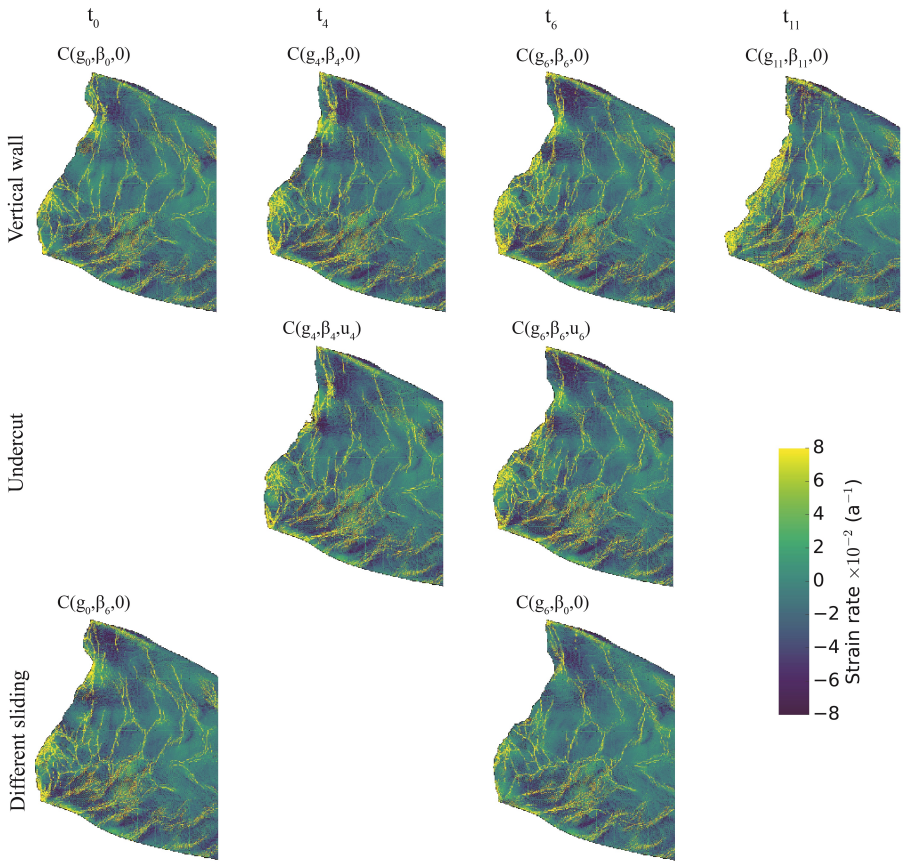

Figure 11. Strain rates modelled with HiDEM for each configuration. Yellow color shows the crevasse pattern and is denser close to the front where the difference between each configuration and time steps can be observed.

advancing (see Fig. 8b) and regardless of the applied modelled front configuration (with or without undercut), a similar slight retreat is modelled. In this case, the undercut has no influence on the calving.

Vertical front configuration at t_6 (red line $C(g_6, \beta_6, 0)$ in Fig. 10c), during a period of accelerated glacier flow, results in slower modelled mean volumetric calving rate ($16.26 \times 10^5\ \mathrm{m^3\ d^{-1}}$) than observed ($26.94 \times 10^5\ \mathrm{m^3\ d^{-1}}$) and no front position change at both SD and ND leading to a mean distance to the observed front close to $60\,\mathrm{m}$. With the undercut configuration (blue line $C(g_6, \beta_6, u_6)$ in Fig. 10b), modelled mean volumetric calving rate ($23.60 \times 10^5\ \mathrm{m^3\ d^{-1}}$) is similar to observation and the front positions at discharge locations are reproduced even though the undercut only represents $5.2\,\%$ of the observed mean volumetric calving rate. The modelled front is still intensively breaking up south of SD but, at that date, it matches the observed retreat.

At the end of the melt season at t_{11}, when subglacial discharge has ended, the observed front retreats at a rate of $24.99 \times 10^5\ \mathrm{m^3\ d^{-1}}$ despite a frontal basal friction higher than at the last studied time step resulting to an averaged frontal velocity of $2.56 \times 10^5\ \mathrm{m^3\ d^{-1}}$. But as shown in Fig. 5, the sliding velocity is higher (lower basal friction, β_{11}) close to the front than further upglacier. Large

calving events occur at both former discharge locations where the bed elevation is lower than anywhere else. The calving front modelled by HiDEM (red line $C(g_{11}, \beta_{11}, 0)$ in Fig. 10d) manages to reproduce this behaviour but overestimates the retreat for the region in between, where the pattern of high strain rate is also denser (see Fig. 11).

Two configurations vary the friction coefficient, β, to assess the role of sliding in the calving process. If the basal friction is set according to t_6 and the geometry to t_0 (orange line $C(g_0, \beta_6, 0)$ in Fig. 10a), the mean volumetric calving rate exceeds observations by more than a factor of 2 ($16.40 \times 10^5\ \mathrm{m^3\ d^{-1}}$), similar to $C(g_6, \beta_6, 0)$, yet with matching spatial frontal patterns as $C(g_0, \beta_0, 0)$ as well as strain rate distribution with elevated rates close to the calved zones. If the geometry of t_6 is simulated with the basal friction of t_0 (orange line $C(g_6, \beta_0, 0)$ in Fig. 10c), it is striking to notice again that the calved zones are similar to the vertical front configuration at t_6 but the mean volumetric calving rate is similar to the observed one at t_0. High strain rates are less pronounced than with the basal friction of t_6 but concentrated at the same locations.

5 Discussion

5.1 Plume Model and Undercutting

Our plume model uses a fixed, planar ice front to calculate submarine melt rates rather than a time-evolving geometry. This assumption is supported by Slater et al. (2017a), who showed that the shape of the submerged ice front does not have a significant feedback effect on plume dynamics or submarine melt rates. However, the same study suggests that the total ablation driven by submarine melting will increase due to the greater surface area available for melting. To take this effect into account in our undercut model, submarine melt rates are horizontally projected onto the undercut front modelled at the previous iteration.

~~The use of constant ambient ocean properties neglects~~

By using ambient temperature and salinity profiles that do not vary in time, we neglect the inter- and intra-annual variability in Kongsfjorden. This variability ~~may influence the plume through changes in~~ can affect the calculated melt rate in two ways: i) the three-equation melt parameterisation explicitly includes the temperature and salinity at the ice-face, and ii) the ambient stratification affects the ~~ambient density stratification , which affects both the vertical plume~~ vertical velocity and neutral buoyancy height ~~, and the temperature of ambient ocean water, which is linearly related to the melt rate. Due to this, there is some uncertainty in the relative magnitudes of the melt rate over longer time scales~~of the plume. The direct effect of changes in temperature and salinity on the melt equations are well tested. Past studies using uniform ambient temperature and salinity conditions have found a linear relationship between increases in ambient fjord temperatures and melt rates, with the slope of the relationship dependent upon the discharge volume (Holland et al., 2008b; Jenkins, 2011; Xu et al., 2013). Salinity, on the other hand, has been shown to have a negligible effect on melt rates (Holland et al., 2008a). However, with a non-uniform ambient temperature and salinity, the effects of changes in the stratification on the plume vertical velocity and neutral buoyancy are much more complex. The stratification in Kongsfjorden is a multi-layer system, with little or no direct relationship between changes in different layers (Cottier et al., 2005). Therefore, testing cases by uniformly increasing or decreasing the salinity would not be informative for understanding the true effects of inter- and intra-annual variability. The high-computational expense of the plume model used here means that it is not yet feasible to run the model on the timescales necessary to

understand this variability, nor to run sufficient representative profiles to provide a useful understanding of the response. Previous work has suggested that intra-annual changes in the ambient stratification are small enough that plumes are relatively insensitive to these changes (Slater et al., 2017b) and that plume models forced with variations in runoff and a constant ambient stratification can qualitatively reproduce observations (Stevens et al., 2016). For these reasons, we highlight this as a limitation of the ~~short-term variability of the plume-driven melt rate is dominated by changes in discharge during the melt season. This short-term variabilitydetermines the pattern of melt across the terminus and is therefore more significant for terminus morphology~~current implementation, and suggest that this should be addressed in future investigations of plume behaviour. A model based upon one-dimensional plume theory (e.g. Jenkins, 2011; Carroll et al., 2015; Slater et al., 2016) would be less computationally expensive and may ~~address~~ allow some of these limitations ~~; however~~to be addressed. However, such a model would not capture the strong surface ~~gravity~~ currents driven by the plume ~~and therefore would not accurately reproduce the spatial patterns of melt over short time scales which is~~ which are important for the terminus morphology studied here.

For ND (Fig. 8b and d), the undercut is in line with the observed front to a certain extent, particularly for t_4. However, for SD, apart for t_3, no ~~imminent~~ apparent correlation between modelled undercut and observed front location seems to exist. However, Fig. 10 shows that modelling calving with undercut at SD and ND for t_4 and t_6 gives a good fit to observation. The difference in agreement with the observed front position and the modelled calving could possibly be explained by the uncertainty in discharge or the different character of the plume at high and low discharge. The low dependence of calving front position on modelled undercut in situations of low discharge seems to have no major influence on the performance of the calving model. At Kronebreen, the high discharge relative to the shallow depth of the terminus drives strong gravity currents at the surface as water is rapidly exported horizontally away from the plume. The melt rates driven by these gravity currents are significant as shown in Fig. 7, and in some cases dominate over the melt rates driven by the plume at depth. The difference between low and high discharges is therefore slightly counter-intuitive. At low discharges, when maximum melt rates occur at depth, the terminus is more undercut but in a narrower area; meanwhile, at higher discharges, strong undercutting occurs but over a much wider area of the terminus. This suggests that calving behaviour may be very different in these two situations.

5.2 Calving model

~~From our results we can conclude that undercutting by subglacial discharge~~ Because the imposed undercuts are the product of melt during the whole interval between observations, the model results should be treated with caution. Benn et al. (2017) compared HiDEM calving for specified undercuts of different sizes and showed that calving magnitude increases with undercut size. For small undercuts, calving simply removes part of the overhang, but for large undercuts calving removes all of the overhang plus additional ice. The mechanisms are different in each case: low-magnitude calving for small undercuts occurs through collapse of part of the unsupported overhang, whereas high-magnitude calving for large undercuts involves forward rotation of the whole front around a pivot point located at the base of the undercut cliff. The long time-step intervals (11 or 18 days) between the starting geometry and the HiDEM simulation in the present study might therefore bias the results towards higher calving events. Testing this possibility is beyond the scope of the present paper, but remains an important goal for

future research. Despite this caveat, our results compare remarkably well with observations, and yield valuable insights into the calving process.

Firstly, the HiDEM results show that undercutting associated with meltwater plumes is an essential factor for calving ~~at discharge location. During~~ during the melt season (t_4 and t_6)~~, surface~~ . Surface melt leads to the formation of a subglacial drainage system that ultimately ~~evacuates the water in~~ releases the water into the ocean from discharge points at the front of the glacier. Simulations without frontal undercutting at these subglacial discharge locations do not agree well with observed frontal positions and mean volumetric calving rates. In contrast, simulations with frontal undercutting reproduce the retreat reasonably well at these locations~~and~~ , particularly where the discharge is high such as at ND. ~~Nevertheless, higher subglacial discharge leading to increased undercutting does not necessarily result in larger retreat. For example, at t_6 (see Fig. 10c), the high discharge in ND enables a large undercut to be created close to the surface (see Fig. 8d), which ultimately triggers calving. However, the retreat at SD is larger despite lower discharge and smaller undercut (see Fig. 8e). Here the basal velocity is higher than at ND and probably plays a key role in the retreat since, even with a vertical ice front, the glacier retreats. Besides, higher friction, β_0, leads to no retreat at all outlining the key role of basal friction. At t_4, on the other hand, with a similar undercut and higher basal friction, the observed front is advancing and the modelled front with undercut is slightly retreating. There is a fine tuning between basal friction and frontal undercutting magnitudes. At high discharge and high friction location (ND), frontal undercut seems to trigger calving primarily while at low discharge and low friction location (SD), frontal undercut modulates the effects of basal friction on the calving process~~The largest discrepancy between modelled and observed calving is in the region south of SD at t_4. Here, the model predicts calving of a large block, whereas the observed front underwent little change. This largely reflects the rules used for calving in HiDEM: any block that is completely detached from the main ice body is considered as calved, even if only separated by a narrow crack from the rest of the glacier and still sitting at its original position. This is the case for the large 'calved' region south of SD at t4, where the block was completely detached but remained grounded and in situ. If this were to occur in nature, it would not register as a calving event on satellite images. The discrepancy between model results and observations at this locality therefore may be more apparent than real.

~~Moreover, calving modelling at t_0 and t_6 gives insight in the role of sliding and geometry (frontal position and topography) in the calving process. On one hand,~~ Secondly, the ~~spatial distribution of the calved zones and the high strain rate regions are kept with similar geometries but different sliding. On the other hand, simulations with different geometries and similar basal friction show comparable calving rates. In this context, it appears that the geometry controls the calved zones while the basal friction (glacier dynamics) controls the magnitude of calving (calving rate).~~

~~However, at t_{11}, with higher basal friction and no estimated subglacial discharge, hence no modelled undercut, the observed calving rate is still high (24.99~~model results replicate the observed high calving rates at t_{11}, after the end of the melt season when there is no undercutting. At this time, the observed mean volumetric calving rate is 24.99×10^5 ~~) compared to~~ $\mathrm{m^3\ d^{-1}}$, which compares well with the HiDEM rate of $28.50 \times 10^5\ \mathrm{m^3\ d^{-1}}$. These values are much higher than those at the start of the melt season~~. HiDEM manages to reproduce a high calving rate (28.50) without taking neither the varying ocean temperature nor any undercut into account. This could be due to a combination of geometry and higher basal velocity at the front than inland (see~~ , when there is also zero undercutting. This contrast can be attributed to the high strain rates in the vicinity of the

ice front at t_{11}, which would encourage opening of tensile fractures (Fig. ~~5d)leading to~~ 11). In turn, the high strain rates ~~(see~~ result from low basal friction (Fig. ~~11). In turn,~~ 5d), likely reflecting stored water at the glacier bed after the end of the melt season. It is possible that geometric factors also play a role in the high calving rates at t_{11}, because the mean ice front height is greater at that time than at t_0, reflecting sustained calving retreat during the summer months, which would have increased longitudinal stress gradients at the front (Benn et al., 2017). This interpretation is supported by experiments $C(g_0,\beta_6,0)$ and $C(g_6,\beta_0,0)$, in which the ~~basal friction is a result of the basal hydrology of the region. Even when the melt seasonis finished, the drainage system is still influencing the dynamics and the calving. Luckman et al. (2015) showed that frontal ablation rates have the strongest correlation with ocean temperature in the fjord at the season timescale and the correlation with ice velocity appears when velocity is high. Our experiments are not including the varying fjord water temperature and limit our discussion on that subject but the velocity higher at the front than further inland seem in agreement with Luckman et al. (2015)'s results.~~

~~In general, the calving rate is rather well reproduced under suitable conditions (undercut when appropriate and basal friction) apart from the simulation at t_4 where a large region, south of SD, is detached from the glacier in the model while the observed front is not changing. Different hypothesis can be suggested. First, the time between two observations, 26 days, is longer than for the other simulations, 11 days. During the melt season, the velocity can change drastically on a daily basis because of surface runoff and subglacial drainage reorganisation. In this context, the~~ basal friction ~~for that time period is an average and since calving magnitude seems to be directly linked to basal velocity, the model might not reflect the real temporal evolution. In this sense, a smaller timestep could be a solution. However, the simulation at~~ values are transposed for non-undercut ice geometries at t_0 and t_6. Imposing low friction (β_6) at t_0 ~~is also resulting in larger retreat than expected south of SD even though the timestep is smaller (11 days) and the basal friction during this period is not changing much. At~~ produces mean volumetric calving rates similar to (but smaller than) those observed at t_6, ~~this region is actually observed to be calving, reflected by model results. This zone of high strain rates was therefore expected to calve but remained stable until that time while the calving model reproduces this retreat much earlier. Furthermore, in HiDEM, any block that is completely detached from the main ice body is considered as calved, even if only separated by a narrow crack from the rest of the glacier and still sitting at its original position. In this sense, HiDEM may model a calving earlier than observation as milimeter wide cracks would not be considered as calving by observations. In a full coupling, this effect would be neutralised if one is only interested at the accumulated ice loss over the whole season.~~ whereas imposing high basal friction (β_0) at t_6 produces low volumetric calving rates similar to those observed at t_0. The influence of basal friction on calving rates is consistent with the results of Luckman et al. (2015), who found that a strong correlation exists between frontal ablation rates and ice velocity at Kronebreen when velocity is high. Low basal friction is associated with both high near-terminus strain rates and high velocities, facilitating fracturing and high rates of ice delivery to the front. Our experiments do not include varying fjord water temperature, so we cannot corroborate the strong correlation between frontal ablation and fjord temperature observed by Luckman et al. (2015). However, our results are consistent with their finding that melt-undercutting is a primary control on calving rates, with an additional role played by ice dynamics at times of high velocity.

6 Conclusions

In this study, we use the abilities of different models to represent different glacier processes at Kronebreen, Svalbard with a focus on calving during the melt season of 2013. Observations of surface velocity, front position, topography, bathymetry and ocean properties were used to provide data for model inputs and validation.

The long-term fluid-like behaviour of ice is best represented using the continuum ice flow model Elmer/Ice that computes basal velocities by inverting observed surface velocities and evolves the geometry, including the front position. During the melt season, a subglacial hydrology system is created and the water is eventually evacuated at the front of the glacier. We used a simple hydrology model based on surface runoff directly transmitted to the bed and routing the basal water along the deepest gradient of the hydraulic potential. Two subglacial discharge locations have been identified by this approach: the northern one evacuates water with a high rate ($\sim$10-100 $\mathrm{m^3\,s^{-1}}$) and the southern one with a low rate ($\sim$1-3 $\mathrm{m^3\,s^{-1}}$). This fresh water is subsequently mixed with ocean water. Rising meltwater plumes entrain warm fjord water and melts the subaqueous ice creating undercuts at the subglacial discharge location. We modelled the plume ~~in~~ with a simplified 2D geometry using a high-resolution plume model based upon the fluid dynamics code Fluidity adapted to the front height and the ocean properties of Kronebreen. Melt rates depend on the discharge rate and the shape of the plume differs greatly with its magnitude. Higher discharges tend to let the plume rise to the surface close to which melt rates are the highest while low discharges concentrate the melt at lower elevations. The melt rates are then projected to the actual frontal geometry taking into account the subaqueous ice-front shape of the former timestep. It is interesting to note that modelled undercuts for high subglacial discharges are spatially close to the observed calving front whereas such a correspondence is not evident for small discharges. The elastic-brittle behaviour of the ice, such as crevasse formation and calving processes, is modelled using a discrete particle model, HiDEM. ~~A new front position is calculated as well as strain rates.~~

~~Four different~~ Two factors impacting glacier calving are studied here ~~through the calving model: geometry (topography and front position) , basal sliding through basal friction, undercutting created by subglacial discharge and strain rate~~using HiDEM: i) melt-undercutting associated with buoyant plumes; and ii) basal friction, which influences strain rates and velocity near the terminus. The performance of the calving model is evaluated quantitatively by comparing observed and modelled mean volumetric: calving rate and qualitatively by comparing calved regions. Results show that ~~the high strain rate zones calculated by HiDEM seem to match the calved regions controlled by the geometry even under modification of basal sliding. Basal friction, in turn, appears to control the magnitude of the retreat. Modelling undercut appears to be necessary to trigger calving at the subglacial discharge location, particularly at high discharge, but not sufficient as basal friction plays a role on the magnitude of the retreat.~~ modelled calving rates are smaller than observed values during the melt season in the absence of melt-undercutting, and that there is a closer match with observations if undercutting is included. Additionally, there is good agreement between modelled and observed calving before (t_0) and after (t_{11}) the melt season, when there is no undercutting. Both modelled and observed calving rates are much greater after the melt season than before, which we attribute to lower basal friction and higher strain rates in the near-terminus region at t_{11}. The influence of basal friction on calving rates is corroborated by model experiments that transposed early and late-season friction values, which had a large effect on modelled calving. These

results are consistent with the conclusions of Luckman et al. (2015), that melt-undercutting is the primary control on calving at Kronebreen at the seasonal scale, whereas dynamic factors are important at times of high velocity (i.e. low basal friction).

~~This study confirms the controls on calving discussed by Benn et al. (2007) and goes further:~~

1. ~~Geometry (frontal position and topography) controls the high strain rate locations and the calved regions,~~
2. ~~Basal friction (associated to crevasse opening and glacier velocity) controls the calving rate,~~
3. ~~Undercut, associated with geometry, subglacial drainage, and ocean properties, but also to former state of undercutting, controls the melt season calving at subglacial discharge locations, but undercuts created from high discharge have more impact on the calving than from low discharge. High subglacial discharge concentrates the melt close to the water surface while low discharge creates an undercut at lower elevations.~~

~~To be able to perform a full coupling,~~ In this paper, we have shown that one-way coupling of ice-flow, surface melt, basal drainage, plume-melting, and ice-fracture models can provide a good match to observations and yield improved understanding of the controls on calving processes. Full model coupling, including forward modelling of ice flow using a physical sliding law, ~~depending on effective pressure at the bedrock, and consequently a more complex model describing the evolution of the subglacial hydrology, is needed. At this stage, the inversion helps to reproduce observed surface velocities with a given front position. If a new calving front from the model would be implemented, observed velocities would not necessarily match the new geometry.~~ would allow the scope of this work to be extended farther, including prediction of glacier response to atmospheric and oceanic forcing.

Author contributions. DV contributed to the design of the study, the one-way coupling, the development of the undercut model, the Elmer/Ice and HiDEM set-ups and the writing of the manuscript. DB edited the manuscript. All other authors provided comments to the manuscript. JÅ developed the HiDEM model and used Kronebreen as test and development case. AE developed the plume model. TZ contributed to the Elmer/Ice set-up. RP calculated the water discharge. DB and AL provided the observed surface velocity maps. WVP developed the coupled energy balance - snow modelling approach. JK provided the interpolated bed map.

Acknowledgements. We thank CSC - IT Center for Science Ltd. for the CPU time provided under Nordforsk NCoE SVALI. Thomas Zwinger was supported by the Nordic Center of Excellence eSTICC (eScience Tools for Investigating Climate Change in Northern High Latitudes) funded by Nordforsk (grant 57001). Acquisition of the TerraSAR-X imagery was funded by the ConocoPhillips Northern Area Program, via the CRIOS project (Calving Rates and Impact on Sea Level).The leading author received an Arctic Field Grant from the Svalbard Science Forum to acquire radar lines for the basal topography in 2014.

References

Aliani, S., Sciascia, R., Conese, I., D'Angelo, A., Del Bianco, F., Giglio, F., Langone, L., and Miserocchi, S.: Characterization of seawater properties and ocean heat content in Kongsfjorden, Svalbard Archipelago, Rendiconti Lincei, 27, 155–162, doi:10.1007/s12210-016-0544-4, 2016.

Amundson, J. M. and Truffer, M.: A unifying framework for iceberg-calving models, Journal of Glaciology, 56, 822–830, doi:10.3189/002214310794457173, 2010.

Åström, J. A., Riikilä, T. I., Tallinen, T., Zwinger, T., Benn, D., Moore, J. C., and Timonen, J.: A particle based simulation model for glacier dynamics, Cryosphere, 7, 1591–1602, doi:10.5194/tc-7-1591-2013, 2013.

Åström, J. A., Vallot, D., Schäfer, M., Welty, E. Z., O'Neel, S., Bartholomaus, T., Liu, Y., Riikilä, T., Zwinger, T., Timonen, J., et al.: Termini of calving glaciers as self-organized critical systems, Nature Geoscience, 7, 874–878, doi:10.1038/NGEO2290, 2014.

Bassis, J. and Jacobs, S.: Diverse calving patterns linked to glacier geometry, Nature Geoscience, 6, 833–836, doi:10.1038/ngeo1887, 2013.

Benn, D. I., Warren, C. R., and Mottram, R. H.: Calving processes and the dynamics of calving glaciers, Earth-Science Reviews, 82, 143–179, doi:10.1016/j.earscirev.2007.02.002, 2007.

Benn, D. I., Åström, J., Zwinger, T., Todd, J., Nick, F. M., Cook, S., Hulton, N. R., and Luckman, A.: Melt-under-cutting and buoyancy-driven calving from tidewater glaciers: new insights from discrete element and continuum model simulations, Journal of Glaciology, pp. 1–12, doi:10.1017/jog.2017.41, 2017.

Boehme, L., Lovell, P., Biuw, M., Roquet, F., Nicholson, J., Thorpe, S. E., Meredith, M. P., and Fedak, M.: Technical Note: Animal-borne CTD-Satellite Relay Data Loggers for real-time oceanographic data collection, Ocean Science, 5, 685–695, doi:10.5194/os-5-685-2009, 2009.

Carroll, D., Sutherland, D. A., Shroyer, E. L., Nash, J. D., Catania, G. A., and Stearns, L. A.: Modeling turbulent subglacial meltwater plumes: Implications for fjord-scale buoyancy-driven circulation, Journal of Physical Oceanography, 45, 2169–2185, doi:10.1175/JPO-D-15-0033.1, 2015.

Church, J., Clark, P., Cazenave, A., Gregory, J., Jevrejeva, S., Levermann, A., Merrifield, M., Milne, G., Nerem, R., Nunn, P., Payne, A., Pfeffer, W., Stammer, D., and Unnikrishnan, A.: Sea Level Change, book section 13, pp. 1137–1216, Cambridge University Press, Cambridge, United Kingdom and New York, NY, USA, doi:10.1017/CBO9781107415324.026, 2013.

Claremar, B., Obleitner, F., Reijmer, C., Pohjola, V., Waxegard, A., Karner, F., and Rutgersson, A.: Applying a Mesoscale Atmospheric Model to Svalbard Glaciers, Advances in Meteorology, Article ID: 321649, doi:10.1155/2012/321649, 2012.

Cook, S., Zwinger, T., Rutt, I., O'Neel, S., and Murray, T.: Testing the effect of water in crevasses on a physically based calving model, Annals of Glaciology, 53, 90–96, doi:10.3189/2012AoG60A107, 2012.

Cottier, F., Tverberg, V., Inall, M., Svendsen, H., Nilsen, F., and Griffiths, C.: Water mass modification in an Arctic fjord through cross-shelf exchange: The seasonal hydrography of Kongsfjorden, Svalbard, Journal of Geophysical Research: Oceans, 110, doi:10.1029/2004JC002757, 2005.

Darlington, E. F.: Meltwater delivery from the tidewater glacier Kronebreen to Kongsfjorden, Svalbard; insights from in-situ and remote-sensing analyses of sediment plumes, Ph.D. thesis, © Eleanor Darlington, 2015.

Everett, A., Lydersen, C., Kovacs, K. M., Kohler, J., and Sundfjord, A.: Hydrography data from GPS-CTD-SRDL-equipped Ringed seals in Kongsfjorden 2012, doi:10.21334/npolar.2017.7b538020, 2017.

Fried, M., Catania, G., Bartholomaus, T., Duncan, D., Davis, M., Stearns, L., Nash, J., Shroyer, E., and Sutherland, D.: Distributed subglacial discharge drives significant submarine melt at a Greenland tidewater glacier, Geophysical Research Letters, 42, 9328–9336, doi:10.1002/2015GL065806, 2015.

Gagliardini, O., Zwinger, T., Gillet-Chaulet, F., Durand, G., Favier, L., de Fleurian, B., Greve, R., Malinen, M., Martín, C., Råback, P., Ruokolainen, J., Sacchettini, M., Schäfer, M., Seddik, H., and Thies, J.: Capabilities and performance of Elmer/Ice, a new-generation ice sheet model, Geoscientific Model Development, 6, 1299–1318, doi:10.5194/gmd-6-1299-2013, 2013.

Gillet-Chaulet, F., Gagliardini, O., Seddik, H., Nodet, M., Durand, G., Ritz, C., Zwinger, T., Greve, R., and Vaughan, D. G.: Greenland ice sheet contribution to sea-level rise from a new-generation ice-sheet model, Cryosphere, 6, 1561–1576, 2012.

Goldberg, D. N. and Sergienko, O. V.: Data assimilation using a hybrid ice flow model, The Cryosphere, 5, 315–327, 2011.

Holland, D. M., Thomas, R. H., De Young, B., Ribergaard, M. H., and Lyberth, B.: Acceleration of Jakobshavn Isbrae triggered by warm subsurface ocean waters, Nature geoscience, 1, 659–664, doi:10.1038/ngeo316, 2008a.

Holland, P. R., Jenkins, A., and Holland, D. M.: The response of ice shelf basal melting to variations in ocean temperature, Journal of Climate, 21, 2558–2572, doi:10.1175/2007JCLI1909.1, 2008b.

How, P., Benn, D. I., Hulton, N. R. J., Hubbard, B., Luckman, A., Sevestre, H., Van Pelt, W. J. J., Lïndback, K., Kohler, J., and Boot, W.: Rapidly-changing subglacial hydrology pathways at a tidewater glacier revealed through simultaneous observations of water pressure, supraglacial lakes, meltwater plumes and surface velocities, The Cryosphere Discussions, 2017, 1–29, doi:10.5194/tc-2017-74, 2017.

Howe, J. A., Moreton, S. G., Morri, C., and Morris, P.: Multibeam bathymetry and the depositional environments of Kongsfjorden and Krossfjorden, western Spitsbergen, Svalbard, Polar Research, 22, 301–316, doi:10.1111/j.1751-8369.2003.tb00114.x, 2003.

Jarrin, N., Benhamadouche, S., Laurence, D., and Prosser, R.: A synthetic-eddy-method for generating inflow conditions for large-eddy simulations, International Journal of Heat and Fluid Flow, 27, 585 – 593, doi:10.1016/j.ijheatfluidflow.2006.02.006, 2006.

Jenkins, A.: Convection-driven melting near the grounding lines of ice shelves and tidewater glaciers, Journal of Physical Oceanography, 41, 2279–2294, doi:10.1175/JPO-D-11-03.1, 2011.

Jenkins, A. and Bombosch, A.: Modeling the effects of frazil ice crystals on the dynamics and thermodynamics of Ice Shelf Water plumes, Journal of Geophysical Research: Oceans, 100, 6967–6981, doi:10.1029/94JC03227, 1995.

Kehrl, L. M., Hawley, R. L., Powell, R. D., and Brigham-Grette, J.: Glacimarine sedimentation processes at Kronebreen and Kongsvegen, Svalbard, Journal of Glaciology, 57, 841–847, doi:10.3189/002214311798043708, 2011.

Kimura, S., Candy, A. S., Holland, P. R., Piggott, M. D., and Jenkins, A.: Adaptation of an unstructured-mesh, finite-element ocean model to the simulation of ocean circulation beneath ice shelves, Ocean Modelling, 67, 39 – 51, doi:http://dx.doi.org/10.1016/j.ocemod.2013.03.004, 2013.

Köhler, A., Nuth, C., Kohler, J., Berthier, E., Weidle, C., and Schweitzer, J.: A 15 year record of frontal glacier ablation rates estimated from seismic data, Geophysical Research Letters, 43, doi:10.1002/2016GL070589, 2016.

Krug, J., Weiss, J., Gagliardini, O., and Durand, G.: Combining damage and fracture mechanics to model calving, The Cryosphere, 8, 2101–2117, doi:10.5194/tcd-8-1631-2014, 2014.

Krug, J., Durand, G., Gagliardini, O., and Weiss, J.: Modelling the impact of submarine frontal melting and ice mélange on glacier dynamics, The Cryosphere, 9, 989–1003, doi:10.5194/tc-9-989-2015, 2015.

Lindbäck, K., Kohler, J., Pettersson, R., Myhre, P. I., Nuth, C., Langley, K., Brandt, O., Messerli, A., and Vallot, D.: Subglacial topography, geology and implications for future bathymetry of Kongsfjorden, northwestern Svalbard, in preparation, 2017.

Luckman, A., Benn, D. I., Cottier, F., Bevan, S., Nilsen, F., and Inall, M.: Calving rates at tidewater glaciers vary strongly with ocean temperature, Nature communications, 6, doi:10.1038/ncomms9566, 2015.

McNabb, R., Hock, R., and Huss, M.: Variations in Alaska tidewater glacier frontal ablation, 1985–2013, Journal of Geophysical Research: Earth Surface, 120, 120–136, doi:10.1002/2014JF003276, 2015.

McPhee, M. G., Morison, J. H., and Nilsen, F.: Revisiting heat and salt exchange at the ice-ocean interface: Ocean flux and modeling considerations, Journal of Geophysical Research: Oceans, 113, doi:10.1029/2007JC004383, c06014, 2008.

Morlighem, M., Rignot, E., Seroussi, H., Larour, E., Ben Dhia, H., and Aubry, D.: Spatial patterns of basal drag inferred using control methods from a full-Stokes and simpler models for Pine Island Glacier, West Antarctica, Geophysical Research Letters, 37, 2010.

Nahrgang, J., Varpe, Ø., Korshunova, E., Murzina, S., Hallanger, I. G., Vieweg, I., and Berge, J.: Gender specific reproductive strategies of an Arctic key species (Boreogadus saida) and implications of climate change, PLoS one, 9, e98 452, doi:10.1371/journal.pone.0098452, 2014.

Nick, F., Van der Veen, C. J., Vieli, A., and Benn, D.: A physically based calving model applied to marine outlet glaciers and implications for the glacier dynamics, Journal of Glaciology, 56, 781–794, doi:10.3189/002214310794457344, 2010.

Piggott, M. D., Gorman, G. J., Pain, C. C., Allison, P. A., Candy, A. S., Martin, B. T., and Wells, M. R.: A new computational framework for multi-scale ocean modelling based on adapting unstructured meshes, International Journal for Numerical Methods in Fluids, 56, 1003–1015, doi:10.1002/fld.1663, 2008.

Schellenberger, T., Dunse, T., Kääb, A., Kohler, J., and Reijmer, C. H.: Surface speed and frontal ablation of Kronebreen and Kongsbreen, NW Svalbard, from SAR offset tracking, The Cryosphere, 9, 2339–2355, doi:10.5194/tc-9-2339-2015, 2015.

Slater, D., Nienow, P., Goldberg, D., Cowton, T., and Sole, A.: A model for tidewater glacier undercutting by submarine melting, Geophysical Research Letters, 44, 2360–2368, doi:10.1002/2016GL072374, 2017a.

Slater, D., Nienow, P., Sole, A., Cowton, T., Mottram, R., Langen, P., and Mair, D.: Spatially distributed runoff at the grounding line of a large Greenlandic tidewater glacier inferred from plume modelling, Journal of Glaciology, 63, 309–323, doi:10.1017/jog.2016.139, 2017b.

Slater, D. A., Nienow, P. W., Cowton, T. R., Goldberg, D. N., and Sole, A. J.: Effect of near-terminus subglacial hydrology on tidewater glacier submarine melt rates, Geophysical Research Letters, 42, 2861–2868, doi:10.1002/2014GL062494, 2014GL062494, 2015.

Slater, D. A., Goldberg, D. N., Nienow, P. W., and Cowton, T. R.: Scalings for submarine melting at tidewater glaciers from buoyant plume theory, Journal of Physical Oceanography, 46, 1839–1855, doi:10.1175/JPO-D-15-0132.1, 2016.

Smagorinsky, J.: General circulation experiments with the primitive equations, Monthly Weather Review, 91, 99–164, doi:10.1175/1520-0493(1963)091<0099:GCEWTP>2.3.CO;2, 1963.

Stevens, L. A., Straneo, F., Das, S. B., Plueddemann, A. J., Kukulya, A. L., and Morlighem, M.: Linking glacially modified waters to catchment-scale subglacial discharge using autonomous underwater vehicle observations, The Cryosphere, 10, 417–432, doi:10.5194/tc-10-417-2016, 2016.

Straneo, F. and Heimbach, P.: North Atlantic warming and the retreat of Greenland's outlet glaciers, Nature, 504, 36–43, doi:10.1038/nature12854, 2013.

Tarboton, D. G., Bras, R. L., and Puente, C. E.: Combined hydrologic sampling criteria for rainfall and streamflow, Journal of Hydrology, 95, 323 – 339, doi:10.1016/0022-1694(87)90009-6, 1987.

Trusel, L. D., Powell, R., Cumpston, R., and Brigham-Grette, J.: Modern glacimarine processes and potential future behaviour of Kronebreen and Kongsvegen polythermal tidewater glaciers, Kongsfjorden, Svalbard, Geological Society, London, Special Publications, 344, 89–102, doi:10.1144/SP344.9, 2010.

Vallot, D., Pettersson, R., Luckman, A., Benn, D. I., Zwinger, T., Van Pelt, W., Kohler, J., Schäfer, M., Claremar, B., and Hulton, N. R. J.: Basal dynamics of Kronebreen, a fast-flowing tidewater glacier in Svalbard: local spatio-temporal response to water input, Journal of Glaciology (in press), 2017.

Van der Veen, C.: Calving glaciers, Progress in Physical Geography, 26, 96–122, doi:10.1191/0309133302pp327ra, 2002.

Van Pelt, W. J. J. and Kohler, J.: Modelling the long-term mass balance and firn evolution of glaciers around Kongsfjorden, Svalbard, Journal of Glaciology, 61, 731–744, doi:10.3189/2015JoG14J223, 2015.

Xu, Y., Rignot, E., Fenty, I., Menemenlis, D., and Flexas, M. M.: Subaqueous melting of Store Glacier, west Greenland from three-dimensional, high-resolution numerical modeling and ocean observations, Geophysical Research Letters, 40, 4648–4653, doi:10.1002/grl.50825, 2013.